AN ABSTRACT OF THE THESIS OF

Lee E. Collins for the degree of Master of Science in Ocean, Earth, and Atmospheric Sciences presented on October 23, 2013.

Title: Modeling Arctic Melt Ponds Using a Resolved Ice Model with GCM Forcing.

Abstract approved:

Karen M. Shell Eric D. Skyllingstad

The albedo of Arctic sea ice depends greatly on the formation of melt ponds. These ponds form in depressions on the ice as surface snow melts during the summer months, and their location is determined mainly by the initial snow topography. Using a high resolution sea ice model forced with data taken from the Atmospheric Radiation Measurement (ARM) site in Barrow, AK, we investigate how specific factors, both internal model parameters and initial conditions, affect the evolution of melt ponds on Arctic sea ice. We also use forcing data taken from output of the Community Earth Systems Model (CESM) to investigate the differences in melt pond parametrization between our model and CESM. The resolved model uses a unique and innovative approach in pond modeling, the "trigger depth" method, to initiate pond drainage. Results from sensitivity analysis on the trigger depth show the validity of this new approach, suggesting it could be useful in other ice models. The initial snowpack has a very large role in pond formation and extent. We use surface topography gathered from LiDAR scans from the ARM site to provide a realistic snowpack surface. For our sensitivity analysis of the total initial amount of snow in the model, we alter only the minimum thickness of the snow on top of the ice, retaining a consistent surface topography for each simulation. The LiDAR topography from the ARM site provides a more realistic approach to the pond model, as opposed to a randomly generated method of creating snow topography. Large initial snowpack inhibits the formation of deep channels in the ice, reducing pond fraction at the end of the melt season. Finally, we force the resolved model simulations with data from CESM and compare the pond behavior to that of CESM. CESM does an unrealistic

job of representing melt ponds, partially due to the way melt ponds are parametrized in the model, using a “thickness-class” method for creating and categorizing melt ponds. CESM pond formation occurs over a much broader time span compared to observations and our resolved model. Results from this work will be used to investigate and possibly improve the melt pond parametrization in CESM.

Modeling Arctic Melt Ponds Using a Resolved Ice Model with GCM Forcing

by

Lee E. Collins

A THESIS

submitted to

Oregon State University

in partial fulfillment of
the requirements for the
degree of

Master of Science

Presented October 23, 2013
Commencement June 2014

Master of Science thesis of Lee E. Collins presented on October 23rd, 2013.

APPROVED:

Co-major Professor, representing Ocean, Earth, and Atmospheric Sciences

Co-major Professor, representing Ocean, Earth, and Atmospheric Sciences

Dean of the College of Earth, Ocean, and Atmospheric Sciences

Dean of the Graduate School

I understand that my thesis will become part of the permanent collection of Oregon State University libraries. My signature below authorizes release of my thesis to any reader upon request.

Lee E. Collins, Author

ACKNOWLEDGEMENTS

The author expresses sincere appreciation for his advisors, Karen Shell and Eric Skyllingstad. Their unending patience and guiding words made this project possible. The author would also like to thank Chris Polashenski for his collaboration that helped make this work possible. The author also thanks Emily Shroyer and his graduate council representative Michael Lerner for their input on this project. Finally, the author expresses extreme appreciation to all his friends and family for being an incredible support system throughout the entirety of this project.

TABLE OF CONTENTS

LIST OF FIGURES

1 Introduction

Arctic summer sea ice extent has decreased dramatically over the past several decades. New records for minimum September sea ice extent were set in 2005, 2007, and 2012 [Scott and Feltham, 2010] [Fetterer et al., 2002]. In addition, every year since 2002 has recorded a lower minimum sea ice extent than the 1981-2010 average [Fetterer et al., 2002]. Figure 1.1 illustrates the dramatic reduction in sea ice extent between 1980 and 2013.

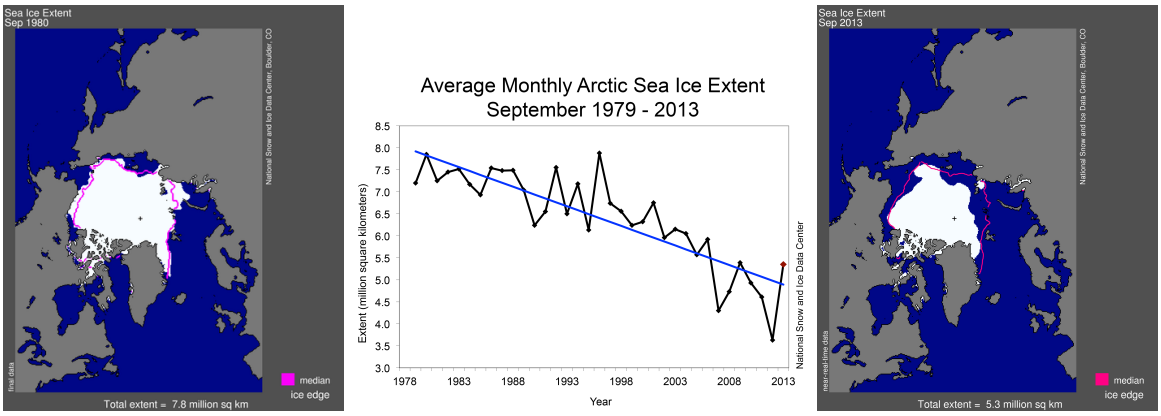

Figure 1.1: *Sea ice extent in 1980 and 2012, as well as the 34 year trend. Total ice extent has decreased from 7.8 million sq. km to 5.3 million sq. km, a 32% reduction.*

Data acquired on submarine cruises from the 1960s to the 1990s shows a reduction in mean sea ice thickness of 1.3m, from an average thickness of 3.1m to 1.8m [Rothrock et al., 1999]. This reduction represents a 40% loss in average sea ice thickness. Satellite observations have shown that not only is the trend of Arctic sea ice extent downward, but it appears to be steepening with time [Ströeve et al., 2012]. Additionally, the Arctic is transitioning from mostly thick, heavily contoured multi-year ice to thin, flat first year ice. During the 1980s, more than 50% of the ice in the Arctic was more than 2 years old, compared to only 25% as of 2011. The amount of

ice 5 years or older has shown an even more significant decline, from 30-40% in the 1980's to only 3% in 2012 [Ströeve et al., 2012]. The implications of the shrinking ice pack include not only regional changes, such as habitat loss for Arctic wildlife and increased coastal erosion, but also global changes such as altered weather patterns in midlatitudes and polar amplification of climate change due to the ice-albedo feedback. Although multi-decadal cycles are responsible for growing and shrinking ice volume to some extent, it is becoming increasingly clear that anthropogenic influences are changing the climate much faster than any natural process. As stated in the 2013 Intergovernmental Panel on Climate Change (IPCC) report: "The reductions in Arctic sea ice extent...are all evidence of systematic climate changes in the cryosphere. All of these changes in the cryosphere have been linked to anthropogenic forcings" [Intergovernmental Panel on Climate Change (IPCC), 2013]. In order to prevent these catastrophic effects, the first step is to better understand Arctic sea ice and how it impacts the global energy budget.

In a steady state, the globally averaged surface temperature of the Earth remains constant, with zero net change in the total energy of the Earth system. All of Earth's incoming energy is provided by the sun, which radiates on the Earth at an annually, globally averaged value of 341 Wm^{-2}. Some of this energy is reflected back into space, while most of the remainder is absorbed by the surface. The Earth's surface emits longwave radiation according to the Stefan-Boltzmann law $F = \sigma T^4$ where F represents the emitted energy flux, σ is the Stefan-Boltzmann constant, and T is the temperature of the planet; this is known as blackbody radiation. An equilibrium surface temperature is obtained when all the incoming solar radiation at the top

of the atmosphere (TOA) is balanced by outgoing longwave radiation emitted by the planet's surface and atmosphere. Any agent that causes a change to this global balance is termed a forcing, and causes the surface temperature to shift until TOA radiative balance is once again restored.

One very important forcing agent is atmospheric CO_2, which is a very effective greenhouse gas. CO_2 selectively absorbs longwave radiation much more strongly than shortwave radiation, allowing incoming solar radiation to pass through the Earth's atmosphere relatively undisturbed, yet blocking and absorbing most of the outgoing longwave radiation emitted by the planet. As it gains energy, the atmosphere emits blackbody radiation of its own according to the Stefan-Boltzmann law described earlier. This radiation is emitted in all directions, including downward towards the planet, causing more energy to be absorbed by the Earth's surface, and resulting in a higher surface temperature. As CO_2 levels in Earth's atmosphere rise, more and more outgoing longwave radiation from Earth's surface is absorbed by the atmosphere, causing the atmosphere to radiate more back toward Earth's surface, and creating a net imbalance in the TOA radiation. Because more radiation is incoming compared to outgoing, the planet's surface temperature increases until it radiates enough to retain equilibrium.

A small amount of greenhouse gasses in Earth's atmosphere are necessary to keep the planet's surface temperature in a tolerable range for life to flourish. Without an atmosphere, the radiating temperature of the Earth would be 255K, far too low to support liquid water, and therefore far too low to support life. However, increasing the amount of greenhouse gasses in the atmosphere too much could cause the

planet to heat up much past this tolerable zone, which could have a number of disastrous consequences, including sea level rise, habitat loss, depletion of Arctic sea ice [Intergovernmental Panel on Climate Change (IPCC), 2013], and an increase in the frequency and severity of natural disasters.

What makes the changing climate so difficult to study and predict are the various climate feedbacks that either amplify or dampen the effects of a climate forcing. A simple example of a climate feedback is the Planck feedback: as the planet warms up, it radiates more longwave energy to space, which thereby results in a reduction in global surface temperature. This is an example of a negative feedback: as CO_2 levels rise and the planet warms, the system emits more longwave radiation, cooling the planet and damping the effects of the original forcing. A positive feedback is exactly the opposite, one that amplifies the effects of the original forcing. One example of a positive feedback is in the effect of water vapor on climate change. As increased CO_2 levels make surface temperatures rise, the amount of water vapor in the atmosphere also increases. Water vapor, as a strong greenhouse gas, selectively absorbs and emits longwave radiation, thereby intensifying the original CO_2 forcing effect, and increasing surface temperatures even more.

Arctic sea ice is extremely sensitive to a warming climate due to the ice-albedo feedback. The albedo of a surface is a unitless number between zero and one representing how reflective that surface is. Albedo is calculated by dividing the amount of radiation the surface reflects by the total incident radiation. Therefore, an albedo of one indicates complete reflectivity, and an albedo of zero represents total absorption. The total globally averaged albedo of the Earth is approximately 0.3 [Trenberth

et al., 2009]. Snow-covered sea ice is one of the most reflective natural surfaces on the planet, with an albedo as high as 0.9 [Polashenski et al., 2012], and contributes to global cooling by reflecting almost all incident sunlight back to space. As the planet warms, some of this ice melts, exposing more open ocean. Open ocean water has a very low albedo of 0.1 [Eicken et al., 2004]. With less ice to reflect incoming solar radiation, and more ocean surface to absorb it, the planet warms even more, melting more ice, and creating a positive feedback effect.

Melt ponds have a large impact on the albedo of Arctic sea ice. A melt pond is simply a pool of liquid water that forms on the surface of the ice as snow melts during the summer months. The albedo of melt ponds can vary between 0.6 and 0.15, drastically lower than the surrounding snow and ice [Skyllingstad et al., 2009]. Over the course of the summer, melt ponds can cover over 50% of the sea ice area, reducing the total albedo of the ice from 0.9 to as little as 0.3. Smaller albedo changes still have the capacity to alter the surface energy budget dramatically, as ice with an albedo of 0.6 absorbs enough energy to melt 2.6cm more ice per day than ice with an albedo of 0.25 [Polashenski et al., 2012]. Because they have the capability of changing the albedo of the sea ice so dramatically, melt ponds are of great interest. Figure 1.2 shows the enormous contrast between the dark surface of the ponds and the bright, white surface of the surrounding snow and ice.

Currently, we use global climate models (GCMs) to predict how the Arctic sea ice pack will change under a variety of forcing conditions. Models are tested by comparing their predictions to actual observed data.For a model to be trusted in extrapolating future conditions, it must at the very least “predict” past observations

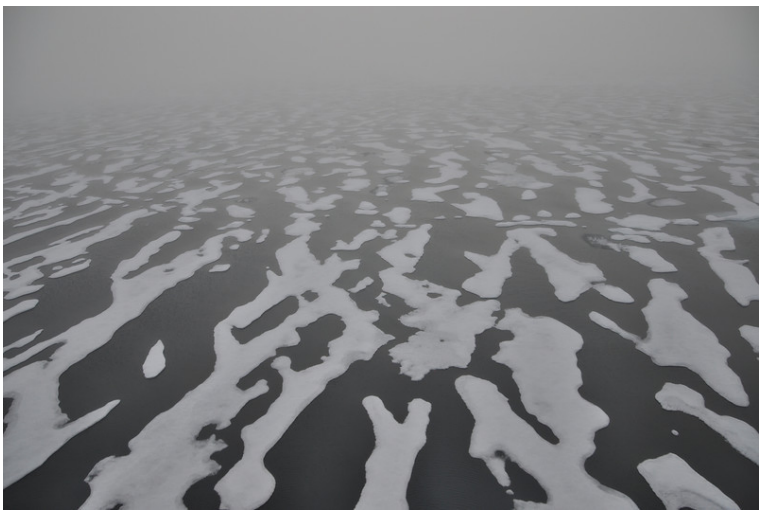

Figure 1.2: *Picture of Arctic melt ponds, showing the dramatic contrast between white, bright ice and dark melt ponds. [Polashenski, 2011]*

correctly. Newer models are showing more consistency with observations from the satellite era [Ströeve et al., 2012], however even the most advanced models lack an accurate parameterization for melt ponds [Bitz, 2010]. Because these large-scale models are unable to resolve individual ponds due to the grid size requirements, the effect of the melt ponds needs to be parameterized, or represented in the model in a simpler way. The GCM that I work with to analyze melt ponds is the Community Earth Systems Model (CESM), however dozens of other GCMs exist, each with its own unique method for simulating the changing climate. Figure 1.3 shows the pond fraction for 14 CESM simulations I created for this project, each representing a different year. The figure shows the extreme interannual variability in pond fraction. For example, the start date of initial pond formation varies on the order of months. In observations, the interannual variability of the exact day when ponds begin to form is rarely over a week [Polashenski et al., 2012]. This discrepancy shows the need for improvement in the parameterization of melt ponds, and I hope to influence the development of

these parameterizations with my work on this project.

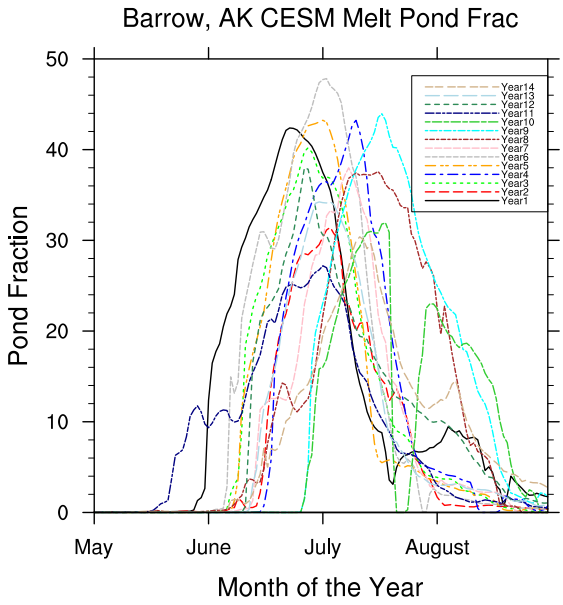

Figure 1.3: *Pond fraction during the melting season for 14 runs of CESM, each representing a different year. A large interannual variability is observed in all aspects of these simulations, including the date at which ponds begin to form, the maximum pond fraction, and the date at which the ponds drain. This interannual variability is not observed in field data, and provides motivation to continue working on improving melt pond parameterization in global climate models.*

Arctic Melt Ponds

Melt ponds form in a very consistent four-stage process that has been observed for many years [Polashenski et al., 2012]. During the freezing season (August-April), wind shapes the snowpack into hills and troughs, much like sand dunes in the desert. As the ice enters the melting season (May-July), melted snow pools in topographical lows on the ice, forming melt ponds. Due to the albedo difference, ponds begin to grow rapidly after they initially form, as they absorb more radiation and heat up

faster than the surrounding ice. Ponds on first-year ice behave quite differently than ponds on multi-year ice. First year ice tends to be much smoother than multi-year ice, creating ponds that are less deep, but span a much larger area.

The first stage of pond formation is characterized by a rapid rise in pond coverage as rising temperatures cause surface snow to melt quickly. As the ice is still very impermeable, meltwater has very few outflow channels and accumulates in depressions in the ice. During this stage, pond coverage can easily spike past 50%, and the albedo can be reduced from 90% to as low as 30%. As this stage results in a very low albedo of the ice, its duration is very important to the seasonal energy balance [Polashenski et al., 2012]. Figure 1.4 demonstrates the transformation that occurs during stage I, as snow and ice is melted and ponds begin to form.

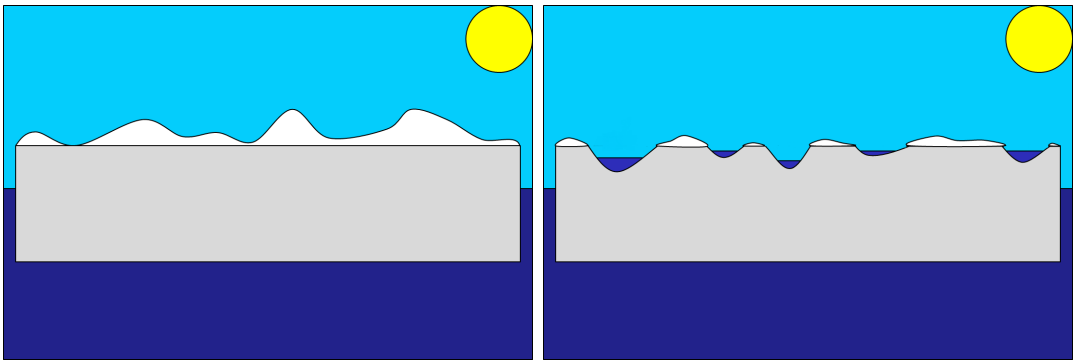

Figure 1.4: *Before(left) and after(right) picture of stage I of melt pond formation. As the snow melts, the meltwater pools in topographic lows, and eventually begins to melt the ice beneath the snowpack.*

In the second stage, the development of macroscopic flaws in the ice, as well as an increase in ice permeability, results in the drainage of ponds to sea level very quickly. Although both sources cause significant water loss, horizontal transport to macroscopic flaws dominates [Polashenski et al., 2012]. This stage is particularly

difficult to model due to the extreme sensitivity of draining to the temperature and permeability of the ice. Figure 1.5 shows how the ponds drain during stage II.

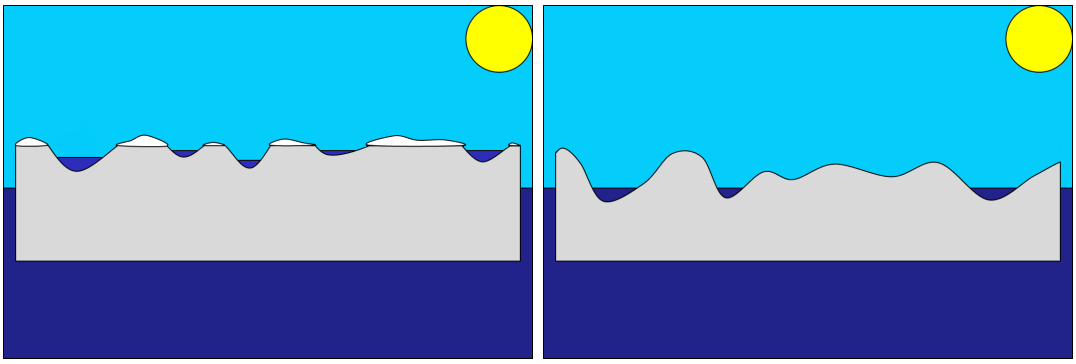

Figure 1.5: *Before(left) and after(right) picture of stage II of melt pond formation. As the ice becomes more permeable, the ponds drain to sea level, leaving ponds only in places where the water table is above the local surface height.*

Ponds stay at or very near sea level in the third stage, as the ice remains permeable enough to allow water to melt through to the ocean. Water is able to drain through the ice with only a slight hydraulic head, and therefore ponds are formed only where the local surface height is below sea level [Polashenski et al., 2012]. As the ice sheet melts and begins to sit lower in the water, more sites with low topography fill with sea water, laterally increasing the total pond area. Although almost all ponds above sea level disappear at this stage, the total pond area slowly increases due to this process. An illustration of this effect is shown in Figure 1.6.

The fourth stage of pond evolution, permanent refreezing, occurs at the end of the melt season, when temperatures fall enough to allow meltwater to freeze and snow to accumulate on top of the ice again. Occasionally freezing can occur earlier if atmospheric forcing causes temperatures to drop and snow to cover the landscape. These events are rare, and last only a few hours, however the albedo change is significant

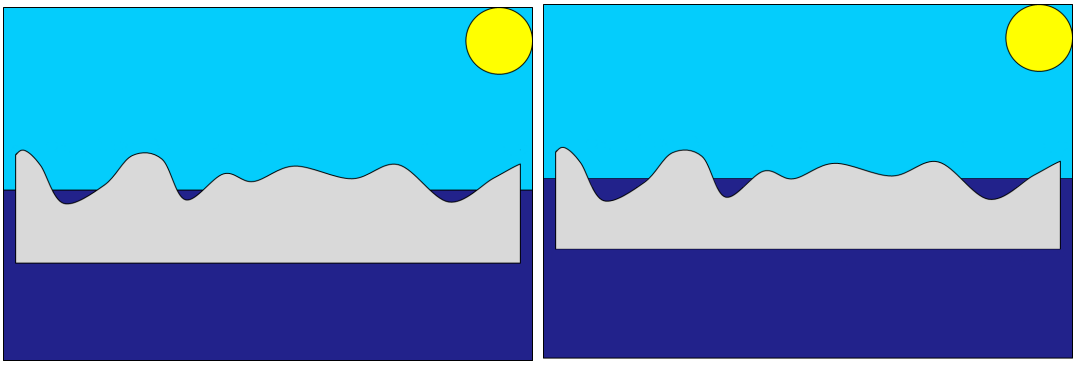

Figure 1.6: *Before(left) and after(right) picture of stage III of melt pond formation. Pond area slowly increases as new ponds form in areas of the ice sheet below sea level.*

enough to greatly alter the surface energy budget, causing much more radiation to be reflected back to space.

Figure 1.7 shows the evolution of pond fraction from observations taken by our collaborator Chris Polashenski near Barrow, AK [Polashenski et al., 2012]. Although the data from 2008 and 2010 is incomplete, the 2009 data clearly shows the first three stages of pond formation. Stage I begins on June 2, as the pond fraction begins to rapidly rise. This stage lasts until June 7, when the pond fraction reaches its peak. Stage II begins just as stage I ends, as ponds drain and the pond fraction declines quickly. This stage ends on June 14, when the pond fraction reaches a local minimum. Stage III then begins and lasts until the end of the data range. Ponds are only present when the local surface height is above sea level during this stage, which is why pond fraction increases much slower during this stage as compared to stage I.

The goal of this project is to understand which factors play the biggest role in melt pond formation, and what effect these factors have on the albedo of the Arctic sea ice. To examine this, I use a very small-scale resolved sea ice model to perform sensitivity analysis on several key parameters of the sea ice system. This model is capable of

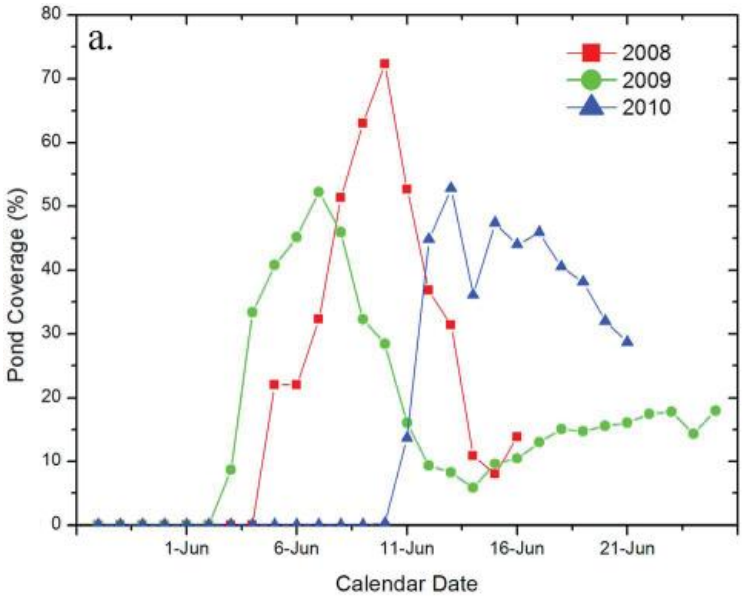

Figure 1.7: *Pond fraction data collected near Barrow, AK. The first three stages of pond evolution are especially apparent in the 2009 data.*

resolving individual ponds separately, something impossible for a large-scale global climate model to accomplish.

To conduct sensitivity analysis on the resolved ice model, I run a series of model simulations, changing several parameters in small increments. The results are analyzed to determine how the selected parameters affect the evolution of melt ponds. Additionally, the model can be tuned using this sensitivity analysis to best pick values for these parameters so the model output matches observations as closely as possible. Finally, I run the model using forcing data from the Community Earth Systems Model (CESM), and compare the output of the resolved model to that of CESM to identify areas where the parameterization of melt ponds in this global climate model can be improved.

2 Methods

Resolved Sea Ice Model Description

The creation of this resolved sea ice model extends previous work reported in Skyllingstad et al. (2007) and Skyllingstad et al. (2009). The current model represents the sea ice and snow more accurately and also simulates how the ponds drain during stage II with a unique approach described later. A complete description of the revised model can be found in Skyllingstad et al. (2013) (in preparation).

The sea ice and snow are represented by a 3-dimensional array, with each grid point containing a value for the temperature, salinity, void fraction (defined as the fraction of empty space in the grid cell), and brine fraction (defined as the fraction of brine, or salty water, relative to the total volume of the grid cell). Surface melting is represented as a change in the void fraction of the top grid point in a vertical column, and the model calculates bottom melting using a simple bulk ocean model with ocean temperature controlled by transmitted solar flux and latent heat flux due to bottom melt. Melt water transport between grid points is calculated using the vertical and horizontal Darcy velocities.

One unique characteristic of this model is the process by which the ponds are triggered to drain at the beginning of stage II. Collaboration with Chris Polashenski revealed that the date at which ponds drain is highly sensitive to the temperature of the ice. As the temperature of the ice increases, it reaches a critical level of permeability at -0.5 °C, which permits the accumulated meltwater to percolate through the ice. In the model, as the trigger depth at a specific grid point reaches -0.5 °C,

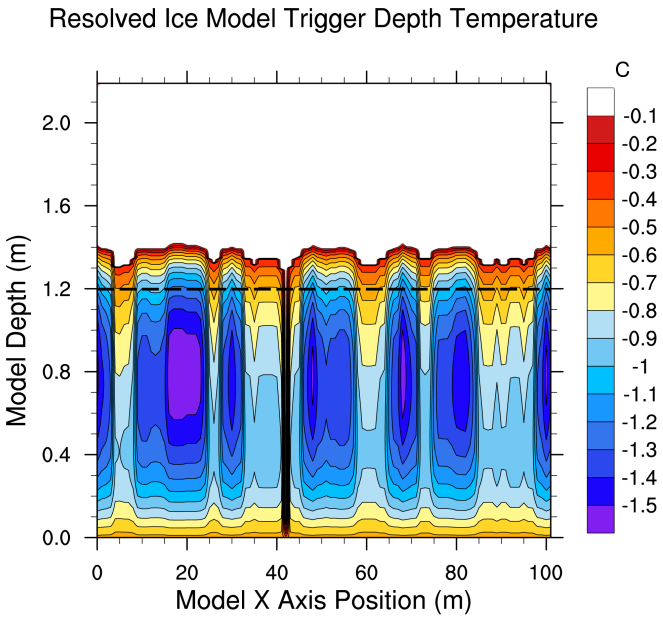

Figure 2.1: *Clarification of the trigger depth mechanism for draining melt ponds. Pictured above is a cross-section of the ice showing the temperature one time step before the ponds are drained. The dotted line shows where the trigger depth is set (20cm below the ice surface). The ponds drain because at this trigger depth, the temperature is exactly -0.5 °C.*

the permeability of the ice at that grid point is increased dramatically, allowing the meltwater to quickly move vertically from the ice surface to the ocean. However, the depth at which to measure this temperature is uncertain. Because the drainage behavior is pivotal to melt pond evolution, this depth parameter, referred to as the trigger depth, was one of the sensitivity parameters studied. Figure 2.1 shows a profile view of the ice one timestep before the ponds drain. The dotted line in the figure represents the trigger depth, showing that the ponds drain just as this depth reaches -0.5 °C.

Sensitivity Parameters

In using this model to perform sensitivity analysis, there are two distinct types of parameters we will be investigating. The first type of parameter represents an initial condition to the model. The initial condition we investigate is the amount of snow on the surface of the ice at the start of the melt season. The resolved ice model uses topographic data collected from field lidar observations near Barrow, AK collected by our collaborator Chris Polashenski [Petrich et al., 2012]. The data is smoothed to a resolution of 0.4m, rotated, and interpolated to a uniform grid using a Barnes objective analysis scheme [Skyllingstad et al., 2013]. The field observations do not include values for the topography of the ice underneath the snow, so we assume that the ice initially has a flat surface and bottom.

To keep the surface snow topography the same for each simulation, the total amount of snow was adjusted by changing the minimum snow depth, which is simply the minimum distance between the surface of the snow and the surface of the ice. Observations indicate that the minimum snow depth in 2009 was 0.01m, and in 2010 was 0.15m. We are interested in the effects of adding even more snow to the surface of the ice. Figure 2.2 illustrates the difference between a high minimum snow depth (10cm) and a very low minimum snow depth (0cm).

The other type of parameter tested using this model is an intrinsic characteristic of the model. One intrinsic characteristic is the trigger depth, discussed earlier. Another example of an intrinsic parameter is the permeability of the ice.

The permeability of the sea ice is a characteristic that determines how quicky

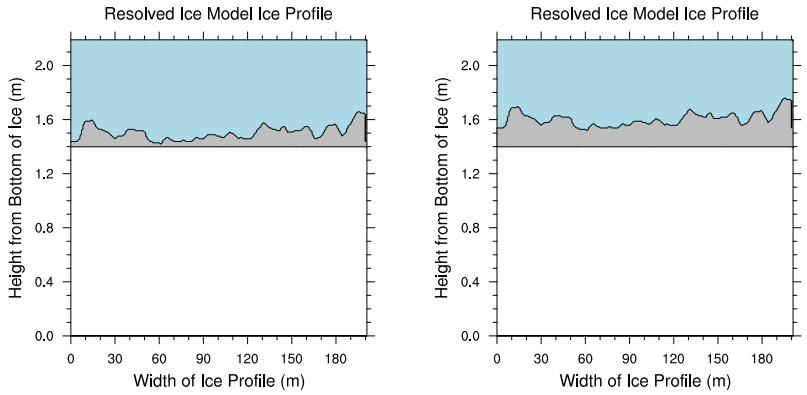

Figure 2.2: *Initial snow cross-sections for a low minimum snow depth (0cm, left) and a high minimum snow depth (10cm, right). The surface topography is identical in both cases; the only difference is the distance between the snow and the ice surface.*

water can be transported through the ice. It is represented by the variable π_v in the vertical Darcy velocity equation [Scott and Feltham, 2010]:

$$v = -\pi_v \frac{g\rho_m}{\mu} \frac{y}{H} \tag{2.1}$$

where g is gravitational acceleration, ρ_m is the density of meltwater, y is the hydraulic head between the pond surface and sea level, μ is the dynamic viscosity of water, and H is the ice thickness.

The accepted value for ice permeability ranges in literature over several orders of magnitude. Proposed values have been between $10^{-7}m^2$ [Freitag and Eicken, 2003] and $10^{-12}m^2$ [Eicken et al., 2004], so our goal in analyzing the permeability was to test this range of values to see which value matched observations the closest. Also, we were particularly interested in how the permeability affected the minimum pond fraction at the end of stage II. Observations show that this minimum pond fraction

rarely dips below 0.10 [Polashenski et al., 2012]; however prior to investigating the permeability, all model runs produced a minimum pond fraction of nearly 0. Our hope was to better replicate the observed minimum pond fraction by testing a range of permeability values.

Based on the semiemperical parameterization introduced by Golden et al. [Golden et al., 2007], the vertical permeability in the resolved sea ice model is proportional to the cube of the solid volume fraction of the ice (ϕ):

$$\pi_v = C(1-\phi)^3 \tag{2.2}$$

For the sensitivity analysis we varied this coefficient C between 10^{-9} and $10^{-11}m^2$. With ϕ of the ice ranging in our model between 0.6 and 0.8, this creates a range in π_v from 10^{-11} to 10^{-13}.

Resolved Ice Model Simulations

Before sensitivity analysis could be performed on the resolved sea ice model, the model was run using standard values to check whether the output followed the traditional stages of melt pond evolution. The first three stages of melt pond evolution are pictured in Figure 2.3, with a rapid rise in pond fraction starting on day 25, drainage on day 35, and slow increase in pond fraction as the freeboard depth increases until the simulation ends.

Comparison of the model results to field data also included a look at the albedo as a function of the pond fraction, shown in figure 2.4. Analysis of several simu-

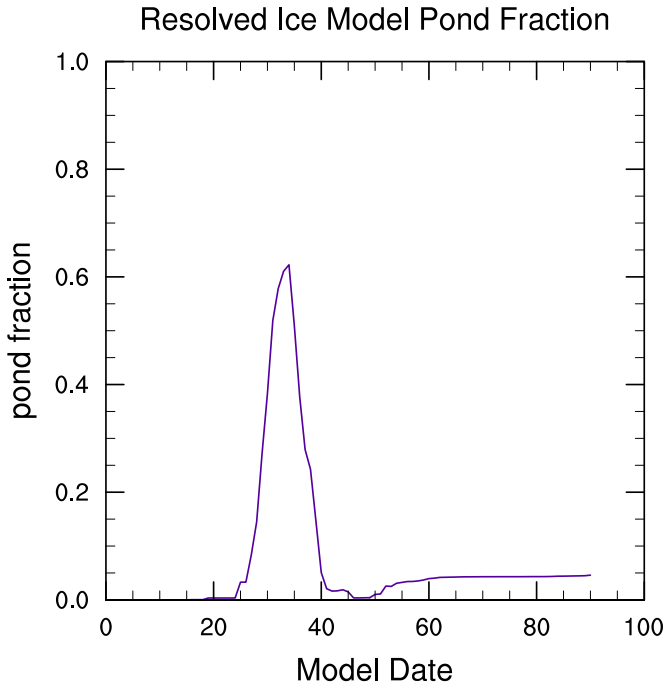

Figure 2.3: *Domain-average pond fraction evolution for a simulation with minimum snow depth = 2cm, trigger depth = 21cm, and permeability constant =* $10^{-10}m^2$*. Stage I begins on day 25, stage II begins on day 34, and stage III begins on day 49, corresponding to calendar dates June 1, June 9, and June 24 respectively.*

lations showed a very clear linear, negative relationship between pond fraction and albedo using a linear least-squares regression, nearly identical to the observed data [Polashenski et al., 2012] [Eicken et al., 2004]. The slope of our model's regression is -0.51, and the slope of the observation regression line is -0.56. Many of the model data points were late in the simulation, when the pond fraction was very near zero. The observed data was never collected this late in the season, and, by removing the 30 points after day 60 from the model, we alter the correlation even closer to the Polashenski data. The similar regression coefficients of our model and the observations gives us reassurance that the dependence of surface albedo on pond fraction in our model is realistic.

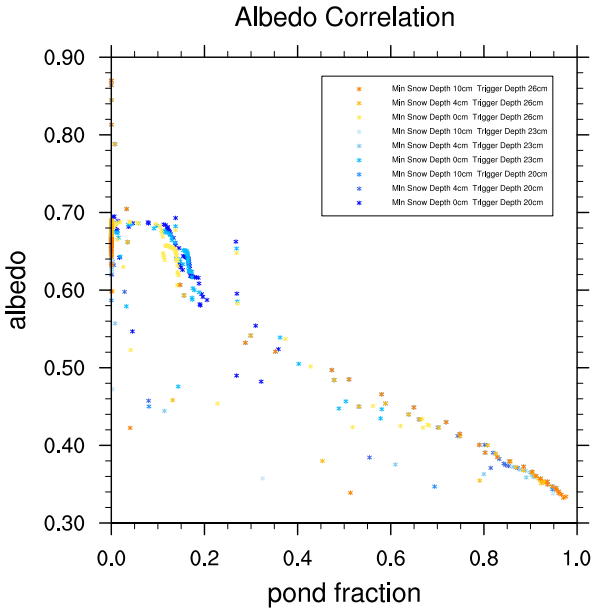

Figure 2.4: *Correlation of domain-averaged albedo and pond fraction for several resolved ice model simulations, indicated by the difference colors.* R^2 *= 0.833 and slope = -0.51. Each point corresponds to one timestep.*

Model Specifications

The model resolution was set at 5cm x 5cm, which allowed an 80 day simulation to be run in approximately 20 hours. Several attempts were made to speed the model up by adding parallelization, using OpenMP to branch time-intensive loops onto multiple processors. Unfortunately the main loop, which calculated fluxes between grid cells, was not able to be parallelized due to memory allocation issues, and the collective effect of parallelizing all the other loops amounted to reducing runtime by several minutes, hardly worth the extra effort. Therefore, parallelization of the program was eliminated in favor of allocating each model run 2 processors per node instead of 8, allowing 4 runs per node to be submitted, or 96 total simulations to be run simultaneously. Although this solution did not reduce the runtime of each simulation, this allowed us to efficiently run sensitivity analysis on multiple parameters at once.

Also, before testing could begin, several minor modifications to the code were required to perform sensitivity analysis. First, the parameters we wanted to investigate were re-coded to be set from a command line variable, instead of hard-coding them into the program. Also, the output file names were re-coded to reflect the value of the sensitivity parameters measured. Finally, several bash scripts were written to allow many simulations to be submitted simultaneously.

CESM Simulations

The Community Earth Systems Model (CESM) is a large-scale global climate model. We wish to compare results from our resolved model to results from CESM in order to identify any similarities or discrepancies in how CESM parameterizes melt ponds. In preparation to run many years of consecutive CESM simulations, much work was done configuring and testing the CESM code to determine the correct resolution and parallelization settings on the computer cluster to maximize runtime efficiency without causing errors. After experimentation, we were able to run the model using a 0.47x0.63 degree atmospheric resolution and a 1 degree ocean/ice grid resolution. The model was run using all fully active components: atmosphere, ocean, land, sea, and ice. Also, the model was forced using present-day CO_2 forcing.

With the ability to run CESM on a powerful cluster of 24 nodes, each with 8 processors per node, we were able to allocate 64 tasks to each component of the model with plenty of room to spare on the cluster. This configuration allowed each simulated year, resubmitted every 3 months, to be completed in less than 3 days.

The first run of CESM was a long-term simulation to gather information about the seasonal variability of the Arctic sea ice, shown in Figure 1.3. This simulation was run for 14 years, writing to the history file daily averaged values for each component, as well as hourly averaged values for the first six years to create the output files necessary to force our resolved sea ice model.

To create the forcing dataset for the resolved sea ice model, the following variables were extracted from the CESM history files:

- air temperature
- wind speed
- surface pressure
- solar zenith angle
- shortwave downwelling solar flux
- longwave downwelling solar flux
- calendar date

The sea ice model natively imports forcing data with a 15min temporal resolution, therefore each of these variables was linearly interpolated to generate data 15 minutes apart. Finally, the data set was spliced to start on May 15th and set to run for 80 days.

To pick the grid point from which to extract the CESM forcing data, we first looked at the grid point closest to Barrow, AK (71.5N, 156W), where the observations were

taken by Chris Polashenski. However, the behavior of the melt ponds at this point did not fit with observations, leading us to believe that this point was too close to land. Upon further inspection, the ice at this point was retreating much faster than observed. Looking at a plot of the surrounding area, this grid point drops to less than 20% ice by the end of each year's melting season.

We believed that moving North, away from the influence of land, would give better results, and therefore we analyzed grid points on the same degree of longitude, but further North from Barrow, until a grid point 3 degrees North of Barrow contained ice that remained above 50% throughout the simulation, enough to give correct pond fraction data. This was the point we selected to use for the forcing data on our resolved ice model.

3 Sensitivity Analysis

With the resolved ice model complete, the main processes in the formation and drainage of melt ponds are represented well in the model. However, several parameters, such as minimum snow depth, trigger depth, and permeability, still exist that are not as well constrained as the rest of the model and can be adjusted to tune the model until it matches the observed behavior. Therefore, we conduct sensitivity analysis on the model to change a few parameters in small increments and analyze the results of these small alterations. This analysis indicates how the model responds to these changes and allows us to pick the values of these parameters that match the observed behavior most closely. We then use these optimal parameter values for the

simulations forced with output from CESM.

We perform sensitivity analysis simulations in two main batches. First, for a constant permeability coefficient ($10^{-9}m^2$), we vary the minimum snow depth and trigger depth. Second, for a constant minimum snow depth (0cm), we varied the trigger depth and permeability constant.

We explore the sensitivity of the minimum snow depth and the trigger depth together first, identifying the effects of both parameters on the metrics defined earlier. We submit 70 runs, with 10 minimum snow depths ranging from 0cm to 20cm, and 7 different drainage trigger depths ranging from 20cm to 26 cm in increments of 1cm. Specific values for the minimum snow depths tested are: 0, 2, 4, 4.5, 5, 5.5, 6, 8, 10, 20cm.

Second, we explore the sensitivity of trigger depth and permeability together. We submit 35 runs, with 7 drainage trigger depths ranging from 20cm to 26 cm in increments of 1cm, and 5 permeability coefficients ranging from $10^{-9}m^2$ to $10^{-11}m^2$, in increments of $5\dot{1}0^{-11}m^2$.

Optimal Ice Model Parameter Values

To pick default values of our sensitivity parameters for the CESM-forced simulations, we look at a set of metrics in each sensitivity run, and compare these metrics to the observed melt pond data from Chris Polashenki. These metrics are:

- Date at which ponds begin forming
- Maximum pond fraction before ponds drain

- Minimum pond fraction after the ponds drain
- Date at which the ponds drain
- Final pond fraction at the end of the melt season
- Minimum ice thickness at the end of the melt season

Matching all of these metrics to the observational data is impossible. Because we wish to match the shape of the melting curve, as opposed to the dates of specific events, we preferentially tune the model to match metrics such as maximum pond fraction and end-date pond fraction, and less importance is placed on metrics such as the initial melt date and drainage date.

Figure 3.1 shows the pond fraction at the end of the simulation for each sensitivity case. The end-date pond fraction according to observations is around 0.10. For reasons discussed in much further detail later, this model shows very little end-date pond fraction for any case except the 0cm minimum snow depth case. Therefore, we can cautiously assume a good value for the minimum snow depth is 0cm.

Figure 3.2 shows the maximum pond fraction for each sensitivity case. According to the observations, the maximum pond fraction should be around 50%. Combining this value with the minimum snow depth from earlier (0cm), this suggests that the drainage triggering depth should be 21 cm.

The goal of changing the ice permeability was to obtain a better match to the minimum pond fraction after drainage in the observed data. In early versions of the model, minimum pond fraction dips far too low after drainage, almost to zero, whereas

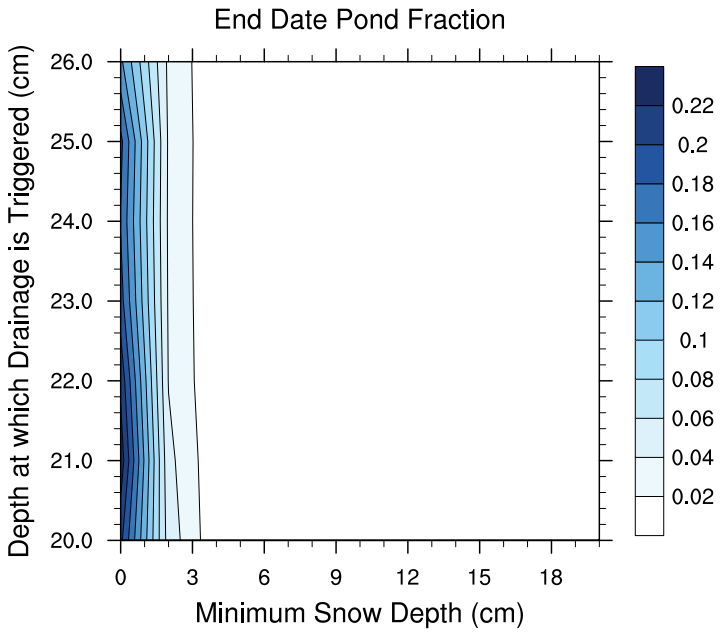

Figure 3.1: *Pond fraction at the end of the simulation for varying minimum snow depth and trigger depth sensitivity parameters using 2009 forcing and topography, with a constant permeability coefficient of* $10^{-9}m^2$.

in the observed data the pond fraction minimum is 10%. Altering the permeability drastically changed the minimum pond fraction. Pictured in Figure 3.3 is a plot of the minimum pond fraction for all trigger depths and ice permeabilities, with minimum snow depth held constant at 0cm.

As previously discussed, the observed data shows a maximum pond fraction of slightly over 50%. Figure 3.4 shows that this pond fraction corresponds to two tested points, permeability coefficient of $5 \cdot 10^{-10}m^2$ and trigger depth of 22cm, and permeability coefficient of $10^{-10}m^2$ and trigger depth of 21cm. The metric we use to pick between these grid points is the minimum pond fraction. Using figure 3.3, the latter grid point (trigger depth=21cm, and premeability coefficient=$10^{-10}m^2$) corresponds better to the observations, as the pond fraction reaches a minimum of 0.1 after drainage according to the 2009 observational data [Polashenski et al., 2012].

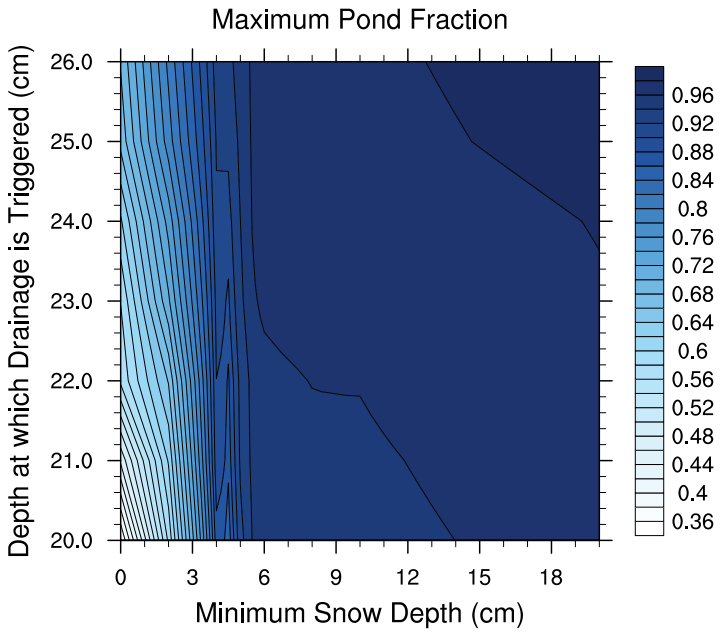

Figure 3.2: *Maximum pond fraction for varying minimum snow depth and trigger depth sensitivity parameters using 2009 forcing and topography, with a constant permeability of* 10^{-9}.

Three other parameters were tested to understand their effects on pond evolution, specifically the effect on the minimum pond fraction after the ponds drain and the start date of ponding. The initial temperature of the snow was adjusted between -8 and 0°C, accounting for the possibility of the snow starting much below 0°C during a particularly cold season. Run with a constant permeability coefficient of $10^{-10}m^2$, trigger depth of 21cm, and minimum snow depth of 0cm (optimal values from the previous section), the initial ice temperature shows no change in start date or minimum pond fraction, and only an 8% change in maximum pond fraction over the entire range of temperatures tested.

Another parameter adjusted was the initial density of the snow. The control value was 0.5 gcm^{-1}, and the sensitivity analysis adjusted the density between 0.4-0.6 gcm^{-1}. As with the initial snow temperature, this parameter had very little effect

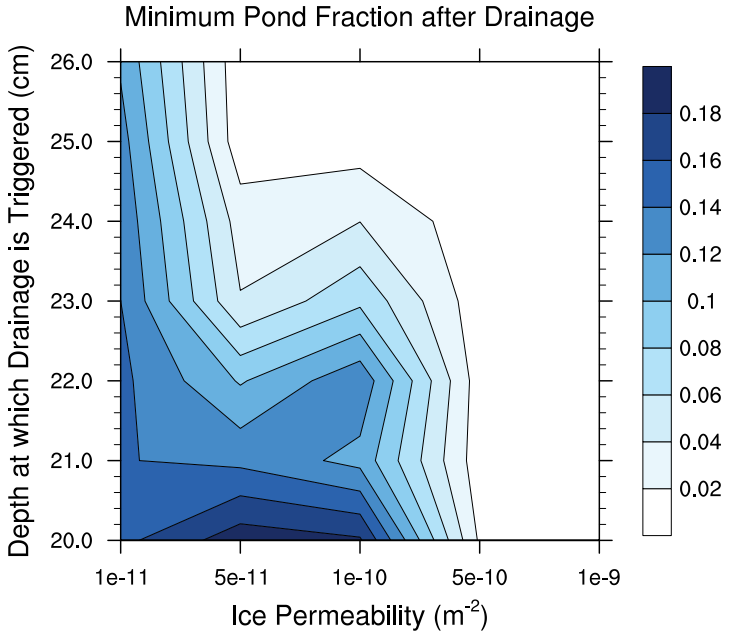

Figure 3.3: *Minimum pond fraction for varying permeability coefficient and trigger depth sensitivity parameters using 2009 forcing and topography, with a constant minimum snow depth of 0cm.*

on the behavior of the melt ponds. Minimum and maximum pond fraction were unchanged, the start date of the melting was concurrent within one day, and the minimum pond fraction remained small.

Finally, the grain size of the snow was varied from $1400\mu m$ to $400\mu m$, investigating the hypothesis that by lowering the grain size, the albedo of the snow would increase and reflect enough incoming radiation to delay the onset of melting by several days. Again, across the entire range of grain sizes, none of the metrics showed any change. Although all of these three attempts revealed interesting information about how these parameters affected the model, none of them were able to replicate the correct starting date of melt pond formation.

Without the time to test more sensitivity parameters, we needed to make some compromises and select values for parameters that created the outcomes we felt were

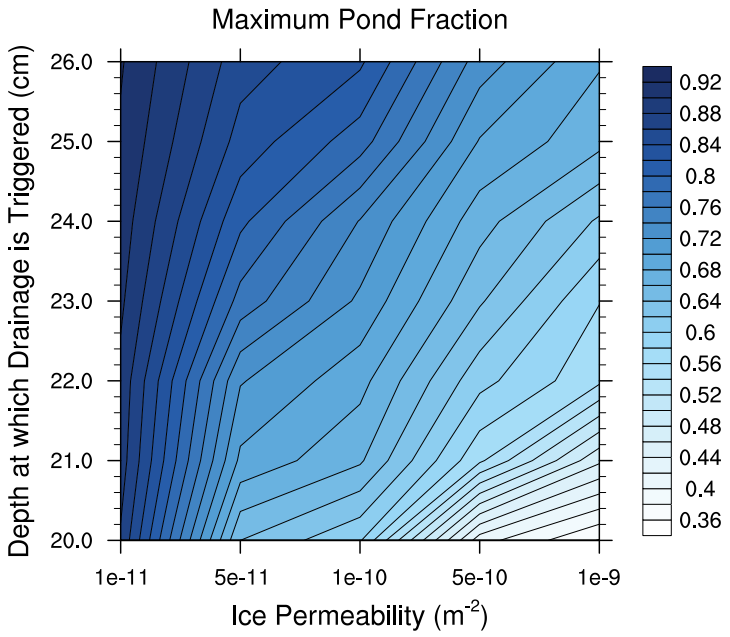

Figure 3.4: *Maximum pond fraction for varying permeability and trigger depth sensitivity parameters using 2009 forcing and topography, with a constant minimum snow depth of 0cm.*

most important. Because we want to match the shape of the melting curve as close as possible to the observed melting curve, we pay most attention to matching metrics such as maximum pond depth and end-date pond fraction, and less importance is placed on dates at which events happen.

We found that a minimum snow depth of 0cm, trigger depth of 21cm, and permeability coefficient of $10^{-10}m^2$ produced model results as close as possible to the observed behavior. With these values determined, we can run the resolved model using CESM forcing and compare the pond fraction output from these runs to pond fraction output from CESM. This will allow us to identify, without any forcing bias, the areas where CESM parameterizes melt ponds well and the areas where CESM could potentially improve.

Minimum Snow Depth

The effect of snow depth on the behavior of melt pond formation is very well studied [Scott and Feltham, 2010], and our results agree with accepted behavior quite well. Based on the results from our sensitivity analysis, increasing the minimum snow depth (MSD) on top of the ice delayed the onset of melting, shown in Figure 3.5. Over the 20cm range of minimum snow depths tested, the onset of melting was delayed by one week. This result corresponds very well with Scott et al. (2010) (pg 16), where a 19cm increase in average snow depth delayed the onset of melting by 9 days past the standard case. Note that our simulations increased the minimum snow depth, and given the different topography of the snow, this may not correspond to an equal increase in the average snow depth.

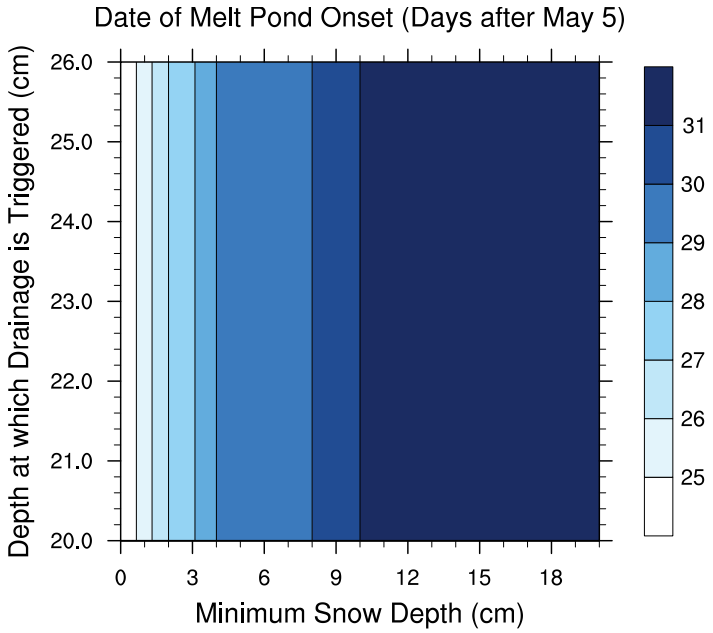

Figure 3.5: *Date of melt pond onset for varying minimum snow depth and trigger depth sensitivity parameters and constant permeability coefficient of* $10^{-9}m^2$*, using 2009 forcing and topography.*

Although the solar forcing input remains constant between simulations, adding additional snow delays the onset of ponding because the simulation takes longer to melt enough snow to form ponds on the ice surface. With identical topography, albedo, and solar forcing, the total amount of meltwater generated each day remains constant for the low MSD and high MSD cases. The difference in the simulations comes when this meltwater is absorbed into the remaining snow in the high MSD case, creating 'slushy snow' and not forming melt ponds. In contrast, this meltwater is immediately formed into ponds in the low MSD case.

Finally, the rate of change of the date of melt pond onset decreases as MSD increases. Onset date is delayed by 3 days between 0cm and 2cm of MSD; however, onset date is only delayed by 1 day between 4cm and 8cm. One possible explanation for this is that wet snow is darker, and absorbs much more solar radiation, than dry snow. Therefore, there may exist a threshold at which the amount of snow packed onto the surface no longer affects albedo, as it all becomes 'dark' after meltwater percolates through it. This is evident when looking at how the albedo changes during the simulation over the range of minimum snow depths tested. Figure 3.6 shows that adding 2cm of snow causes the albedo to decrease much more rapidly and quickly compared to 0cm minimum snow depth at the start of the melt period. Adding 4cm creates a similer effect, although not as pronounced, and adding any more snow does not change the albedo appreciably at all during this rapid melting period. Each case beyond 4cm MSD remains at a similar darkness level, causing the onset date to remain similar for each case. These diminishing returns are most evident with a later run using a minimum snow depth of 20cm. Doubling the snow depth from 10cm to

20cm only adds 1 day to the onset of melting, June 6th instead of June 5th.

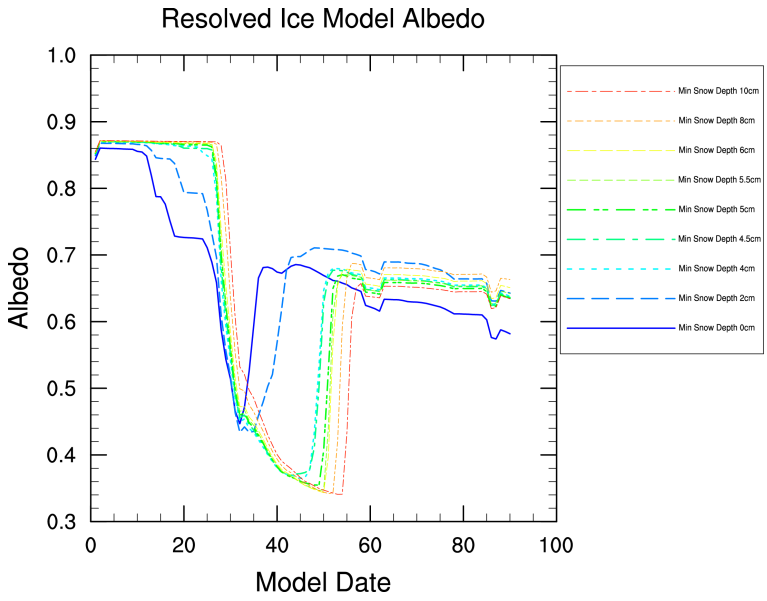

Figure 3.6: *Albedo of resolved ice model simulations with constant trigger depth of 2cm and constant permeability of* 10^{-9}*, using 2009 forcing and topography.*

Along with a delayed onset date of melt pond formation, adding more initial snow also increases the date at which the ponds drain (Figure 3.7. Drainage is triggered in the model when the ice at a specific depth (varied between 20 and 26 cm as the 'trigger depth' sensitivity parameter) reaches -0.5 °C. Therefore, it makes sense that as more snow is accumulated on top of the ice, more time is needed for the additional snow to melt, and therefore increases the time needed to heat the ice down to the trigger depth.

The shift in melting onset date and the shift in drainage date do not coincide perfectly, however. The difference in the date of melt pond onset over the range of the minimum snow depths tested is approximately one week. The range in the date of melt pond drainage is almost 4 weeks. This result is most likely because adding more snow to the surface continues to decrease the rate at which the ice is heated by

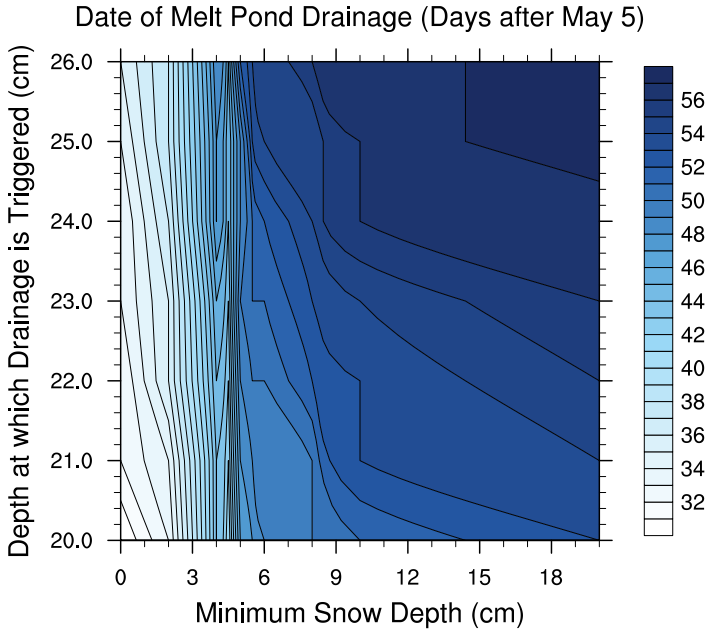

Figure 3.7: *Date of melt pond drainage for varying minimum snow depth and trigger depth sensitivity parameters and constant permeability of* 10^{-9}*, using 2009 forcing and topography.*

requiring more heat to melt the additional snow. Therefore, unlike the onset date of ponding, the drainage date does not reach a level of diminishing returns by adding more snow onto the surface. This result may be a consequence more of the model's coding, and may not be entirely based in reality, as the observational results from Barrow, AK show that in 2010, a year with significantly more initial snow compared to 2009, the delay in drainage date is nearly exactly the same magnitude as the delay in the onset of melting. More research needs to be done to investigate this further.

Another consequence of an increased initial amount of snow on the ice is a drastic increase in the maximum pond fraction before the ponds drain, shown in Figure 3.2, which also corresponds well with Scott et al. (2010) (pg. 16), where an increase of 19cm of snow doubles the maximum pond fraction (note that this study used different snow topography and average snow depth, not minimum snow depth. However, this

study still validates our conclusion that increasing initial snowpack increases the maximum pond fraction). In this model, only about 4cm of added snow depth is needed to double the maximum pond fraction. This dramatic increase is due simply to the added volume of water on top of the ice, which covers almost the entire ice field when melted. The observational data from Barrow, AK shows that the maximum pond fraction for 2008 was much higher than in 2009 [Polashenski et al., 2012]. Using our results from this sensitivity analysis, we would expect a much thicker snow pack in 2008, to result in such a dramatic increase in maximum pond fraction. As expected, according to the Univeristy of Alaska, Fairbanks mass balance site [University of Alaska, Fairbanks, 2012], the average snow depth in Barrow in 2008 was three times the average snow depth in 2009.

One very interesting consequence of this dramatic flooding is the effect on the pond fraction at the end of the simulation, shown in Figure 3.8. Along with a higher maximum pond fraction, more initial snow also corresponds to an extremely diminished pond fraction at the end of the simulation. Based on our simulations, only cases with a minimum snow depth of less than 2cm showed appreciable pond fractions at the end of the simulation. This seems counter-intuitive, as with more initial snow, and more surface meltwater, the ice-albedo feedback should enhance and melt more snow to form more ponds by the end of the season. The answer to this dilemma comes from analyzing the thickness of the ice at the end of the simulation.

We created a metric called the "minimum ice thickness" to understand better why more snow corresponded with a lower end-date pond fraction. Minimum ice thickness is simply the minimum distance between the bottom of the ice and the bottom of a

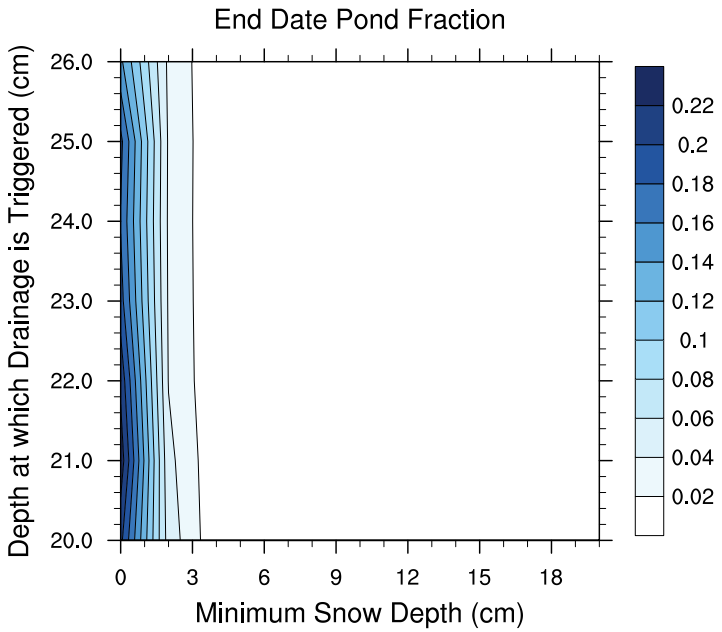

Figure 3.8: *Pond fraction at the end of the simulation for varying minimum snow depth and trigger depth sensitivity parameters and constant permeability of* 10^{-9}*, using 2009 forcing and topography*

pond, looking across the entire ice surface on the last day of the simulation. Figure 3.9 shows the difference between a low minimum ice thickness and a high minimum ice thickness.

Figure 3.10 shows the minimum ice thickness for all values of minimum snow depth and trigger depth tested. There is a very sharp threshold in which the minimum ice thickness at the end of the simulation varies by over twenty centimeters with only a 2.5cm change in the average initial snow depth. To explain this, we must look at the mechanisms by which the late-season pond-fraction is controlled. As is discussed in the introduction, after the ponds drain (at the end of stage II), the only factor that controls the pond fraction is the fraction of ice surface below the freeboard water table. At these points, the water level creates a de-facto pond, as the ice is permeable enough to allow water to percolate through it. Increasing the snow depth at the

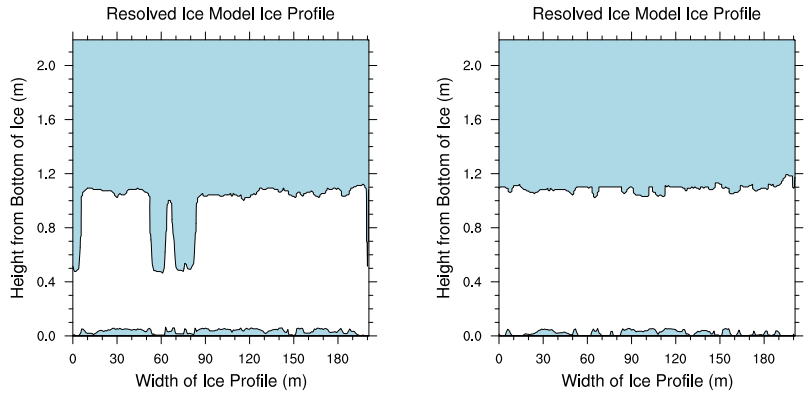

Figure 3.9: *Example of a low minimum ice thickness (0cm, left) and a high minimum ice thickness (6cm, right). These images show a profile view of the ice, with white areas representing ice, blue areas above the ice representing air, and blue areas below the ice representing ocean.*

beginning of the simulation increases the flooding on the surface of the ice, but at the same time inhibits deep channels to be carved, mainly due to the delayed date of pond onset. With melting starting much later, and all the meltwater spread evenly across the ice, the surface of the ice melts much slower and more evenly. Because no early ponds form with a high minimum snow depth, no areas experience rapid early melting due to the ice-albedo feedback. This causes no deep channels to be created in the ice, greatly increasing the minimum ice thickness, shown in Figure 3.10. The threshold in minimum snow depth to trigger this dramatic change in the minimum ice thickness is at 4.5cm in our model. Starting with a snow depth slightly larger, or slightly smaller, than this can cause a change in the deepest pond depth of over 20cm.

The dramatic increase in minimum ice thickness correlates to a reduction in the pond fraction at the end of the simulation due to the dependence of topography on

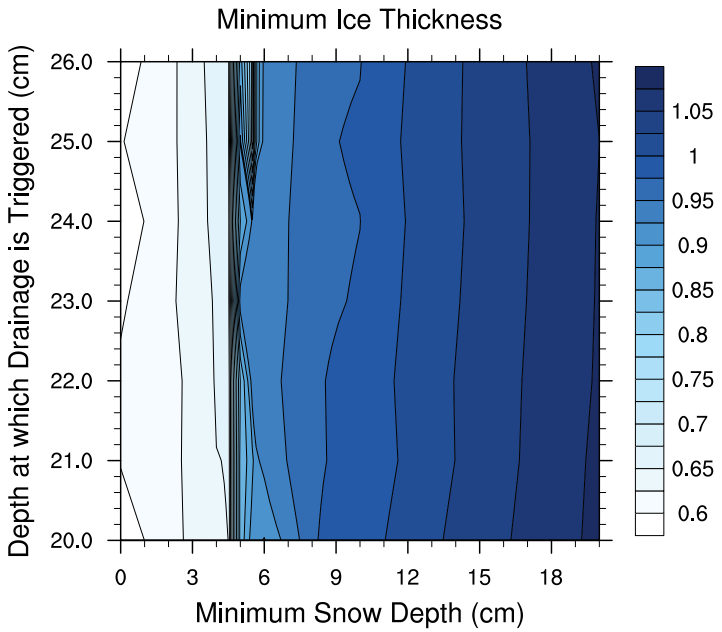

Figure 3.10: *Minimum ice thickness at the end of the simulation for varying minimum snow depth and trigger depth sensitivity parameters and constant permeability of* 10^{-9}*, using 2009 forcing and topography*

end-date pond formation. With a higher minimum snow depth, fewer points on the ice surface exist below the freeboard water table, reducing the total pond fraction. It is worth noting that the minimum snow depth threshold for zero ponding at the end of the melt season is not at 4.5cm, it is between 0 and 2cm. This is mainly due to the minimum ice thickness metric's being an imperfect indicator of how likely ponds are to form at the end of the melt season. Although the minimum ice thickness for the 4cm minimum snow depth case is near 0.65cm, contour plots show that this corresponds to only one pond in the entire domain. So although the minimum ice thickness remains low until a minimum snow depth of 4.5cm, ponds form at the end of the melt season only for minimum snow depths of 0cm and 2cm, because these are the only cases with many deep ponds at the end of the season, not just one or two. Also, it is possible that the initial snow topography affects the probability that pond

form late in the melt season. Large variation in snow depth could cause ponds to form, even with a large minimum snow depth. More research is needed to understand the effects of initial snow topography on the late-season ponding behavior.

The observational data [Polashenski et al., 2012] from 2010 presents contrasting results to this analysis. 2010 had a much deeper snow depth than 2009; however the maximum pond fraction was identical to 2009, and, more importantly, the pond fraction at the end of the melt season did not reach zero, as you would expect with such deep snow. Also, in 2010 snow began to melt almost 20 days later than the 2009 snow, further reducing the time available for deep channels to be carved in the snow which would suggest a lower end pond fraction based on our results. A change in ice thickness between 2010 and 2009 may explain this discrepancy. The 2010 sea ice was noticeably thinner than the 2009 ice, with a thickness of only 1.2m, as compared to 1.4m in 2009. This thinner ice makes it easier for deep enough channels to be carved to dip below the water table, creating ponds after drainage.

The following figures show cross sections of the modeled sea ice at 3 stages of the simulation, day 20, day 45, and day 80. Figure 3.11 is from the 0cm minimum snow depth case, and figure 3.12 is from the 4cm snow depth case. The thick black line shows the air-snow/ice barrier in each case, and the dashed line indicates the water table depth. The depth of the ponds is very clear from these figures, and the two figures show the difference in the depth of the ponds between the low-snow and the high-snow cases. The water table sits at 1m (true water table depth changes throughout the simulation. For simplicity it is represented as the end-date value for these figures), which is able to create ponds in the low-snow case(Figure 3.11 because

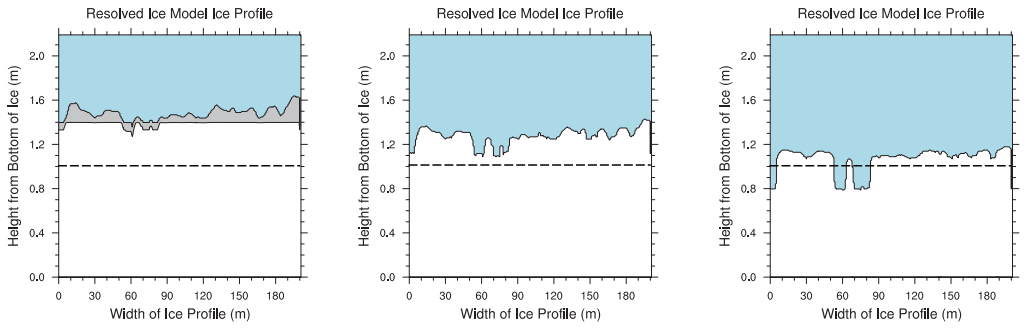

Figure 3.11: *Profile view of the modeled sea ice on day 20(left), day 45(center) and day 80(right). Snow is represented in grey, ice in white and sky in blue. The water table is represented by the dotted line. Minimum snow depth was set at 0cm for this run, and because of the reduced amount of snow at the start, deep channels were able to be carved into the snow by meltwater, allowing ponds to form late in the season as the local water table is above these deep depressions.*

the depressions carved into the ice are deep enough. In the high-snow case (Figure 3.12 however, the channels do not go deep enough to create ponds at the 1m water table depth.

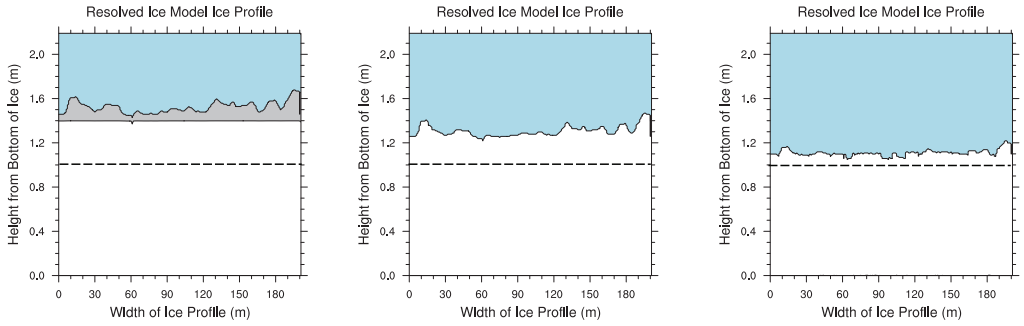

Figure 3.12: *Profile view of the modeled sea ice on day 20(left), day 45(center) and day 80(right). Snow is represented in grey, ice in white and sky in blue. The water table is represented by the dotted line. Minimum snow depth was set at 4cm for this run, and because the snow thickness was higher, deep channels were unable to be carved as they were in the 0cm MSD case. Because no deep channels exist below the water table, the pond fraction at the end of the melt season is negligible.*

Trigger Depth

The second sensitivity parameter that was adjusted was the depth at which we measured the temperature of the ice, such that when the ice reached -0.5 °C, drainage was triggered. Figure 3.13 shows the pond fraction and albedo of model simulations with varying trigger depths, with a constant minimum snow depth of 0cm and permeability constant of $10^{-9}m^2$. One reassuring element of this figure is that the simulations are identical until the time at which the drainage is triggered. Because this was the only part of the model that was modified, while all other factors were held constant, this shows that the model is working properly, and changing the trigger depth should not have any unintended consequences. Because all elements prior to draining are identical for each model run, the onset of melting date is identical for each value of the trigger depth.

Increasing the trigger depth does increase the maximum pond fraction of the model, shown in Figure 3.2 and Figure 3.13. The gradient is strongest with small values for the minimum snow depth, presumably because as more snow is added the pond fraction approaches 100%, and any effect due to an increased trigger depth is difficult to see.

The increase in the maximum pond fraction due to an increase in the trigger depth corresponds to a delay in the drainage date of the ponds. Figure 3.7 shows that across all values of the minimum snow depth, increasing the trigger depth from 20cm to 26cm delayed the date of drainage by about 5 days, enough to cause the maximum pond fraction to double for the smallest minimum snow depth case.

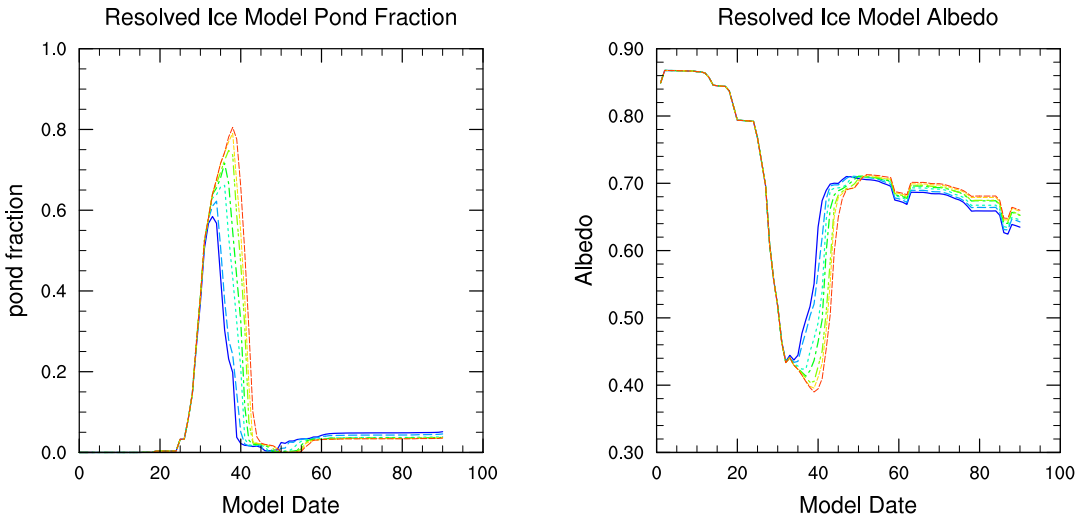

Figure 3.13: *Pond fraction and albedo for several resolved ice model simulations, with a constant minimum snow depth of 0cm, constant permeability of* 10^{-9}*, and a range of trigger depths using 2009 forcing and topography.*

Because the end date pond fraction, shown in Figure 3.8, is most closely controlled by the minimum snow depth (Figure 3.5), this metric was mostly unaffected by the trigger depth. Although extending the ponding phase by an average of 5 days would allow the ice to absorb more heat, and presumably carve deeper ponds, this effect was not pronounced enough to create deep enough ponds below sea level at the end of the simulation. Therefore, all cases except those with the lowest minimum snow depth still had zero pond fraction at the end of the simulation. Indeed, in all cases except for the smallest minimum snow depth, the largest change in minimum ice thickness across all values of the trigger depth was less than 1cm, far too little to cause any appreciable ponding at the end of the simulation. The largest change in minimum ice thickness over all the trigger depths for a constant value of minimum snow depth

was 5cm.

Changes to the trigger depth affect stage I of melt pond evolution the most. By delaying the date at which the ponds drain, the maximum pond fraction increases by a factor of two due to the increased amount of meltwater on the surface of the ice. Stages II and III are unaffected by the trigger depth; the minimum snow depth has the most impact on the minimum pond fraction after the ponds drain, as well as the end-date pond fraction.

Permeability

Permeability of Arctic sea ice is one parameter that is highly uncertain according to current literature, often varying by over 5 orders of magnitude between sources. Because the permeability of the ice affects the behavior of the system mainly during and after pond drainage, the date of pond onset is not affected by permeability, and remains constant at June 1st for each model run.

A smaller magnitude of permeability constant, not surprisingly, leads to greater maximum pond fraction (Figure 3.14), as the meltwater takes longer to drain through the ice. Indeed, as the permeability constant reaches $10^{-13}m^2$, a more extreme value than found in the literature, the ponds never drain, and the simulation stays at near 100% pond fraction until it ends. Note, however, that this value is outside of the values proposed in the literature, and was a test case for the model. This value was not used for any other analysis in this project.

The relationship between the maximum pond fraction and the permeability (Fig-

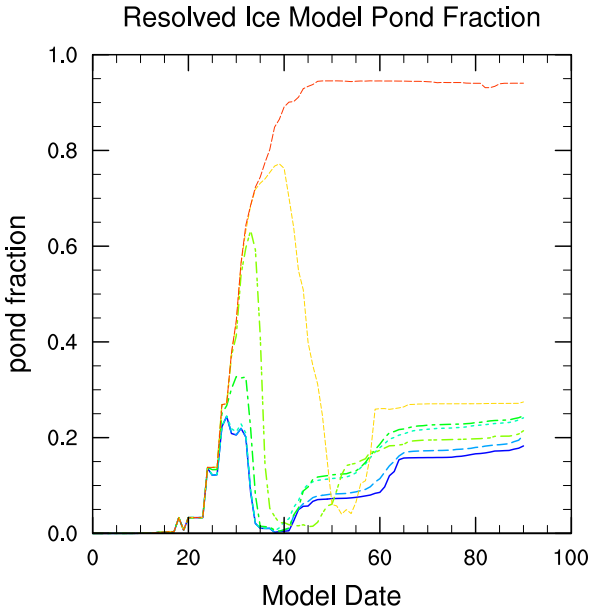

Figure 3.14: *Pond fraction for several resolved ice model simulations with constant trigger depth = 23cm, minimum snow depth = 0cm, using varying permeabilities. These simulations were run using 2009 forcing and topography.*

ure 3.15 is close to logarithmic (due to the exponential x-axis of Figure 3.15), although the gradient is strongest at low trigger depth, since ponds drain earlier when there is less meltwater. At the smallest trigger depth, the range of permeabilities tested ($10^{-9}m^2 - 10^{-11}m^2$) causes the maximum pond fraction to increase by 0.50, whereas at the largest trigger depth, the maximum pond fraction increases by 0.24.

Interestingly, the permeability plays a large role in determining the date at which the ponds begin to drain. Across all trigger depths, the full range of permeabilities causes the date of drainage to be delayed by over 2 weeks, as shown in Figure 3.16. Also, for a constant permeability, the maximum change in the date of melt pond drainage over the range of trigger depths is only 5 days, and the trigger depth becomes more important to this metric as the permeability constant increases. As the permeability of the sea ice decreases, meltwater takes longer to percolate through

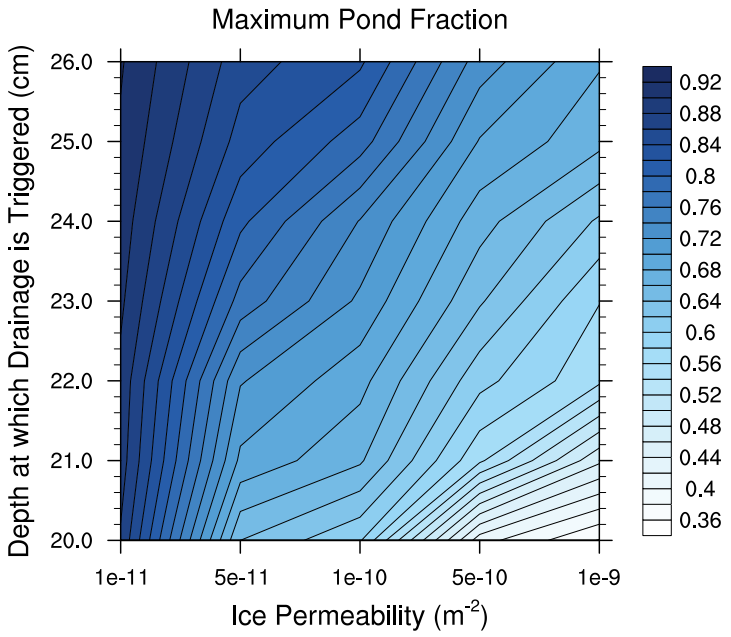

Figure 3.15: *Maximum pond fraction for varying permeability and trigger depth sensitivity parameters and constant minimum snow depth of 0cm, using 2009 forcing and topography.*

flaws in the ice. This may affect the drainage date by limiting the heat flux through the ice due to conduction by meltwater. With less heat allowed to conduct through the ice, the trigger depth takes longer to reach -0.5 °C, and thus the model takes longer to initiate drainage. This may be the most important consequence of a higher permeability constant, as once the ponds are triggered to drain, the pond fraction drops to zero within 1-2 days, regardless of the permeability of the ice.

Along with the maximum pond fraction, the permeability of the ice is also strongly correlated with the pond fraction at the end of the simulation, as seen in Figure 3.17. As we already have determined, for a constant permeability, the end-date pond fraction is controlled mainly by the minimum ice thickness, shown in Figure 3.18. Comparing Figure 3.17 with Figure 3.18, we see the opposite of what is expected: an increase in end-date pond fraction correlates with an increase in minimum ice

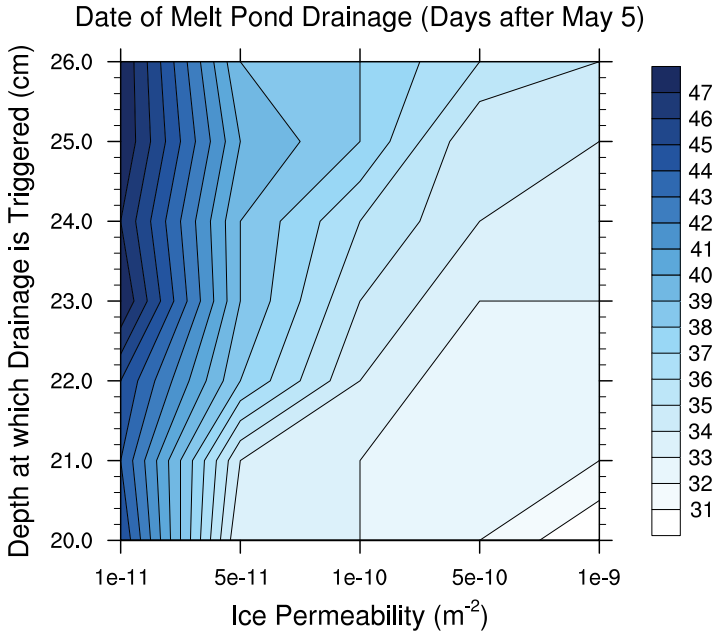

Figure 3.16: *Date of melt pond drainage for varying permeability and trigger depth sensitivity parameters and constant minimum snow depth of 0cm, using 2009 forcing and topography.*

thickness.

This difference could be explained by the increase in drainage date that is accompanied by an decrease in permeability (Figure 3.16). Presumably, as the permeability is decreased, the meltwater is allowed to sit on top of the ice for longer before draining, which causes deeper ponds to be created as the ice-albedo feedback lasts for several more days. It is worth noting that the difference in minimum ice thickness, shown in Figure 3.18, is very small for the range of permeabilities and trigger depths tested, only varying by 1cm across all simulations. This makes it difficult to be certain about any conclusions drawn from this data, although it is clear that minimum ice thickness is not the only parameter that is important in determining end-date pond fraction.

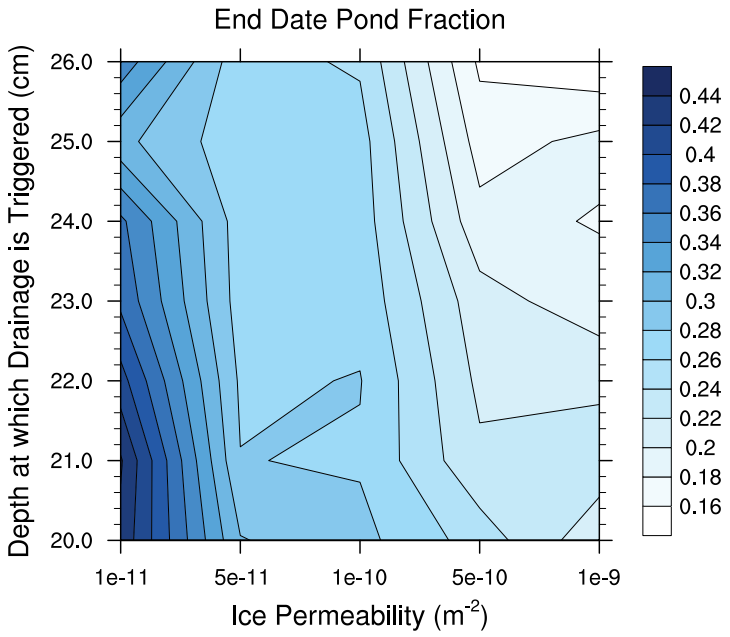

Figure 3.17: *Pond fraction at the end of the simulation for varying permeability and trigger depth sensitivity parameters and constant minimum snow depth of 0cm, using 2009 forcing and topography.*

CESM Forced Simulations

Figure 3.19 shows the results of four resolved model simulations forced using output from four years of CESM simulations, compared with results from the CESM model runs themselves. The figure compares both pond fraction (red lines) and absorbed shortwave radiation (blue lines). The resolved ice model (solid lines) shows the familiar three stages of pond evolution. The sharp melting peak is evident in all four years, although the maximum pond fraction does not peak as high as in the simulations with observational forcing.

The results from CESM (Figure 3.19 dotted lines) show an entirely different representation of ponding. The time between the onset of melting and when the model reaches its minimum pond fraction is much longer than the resolved model. The

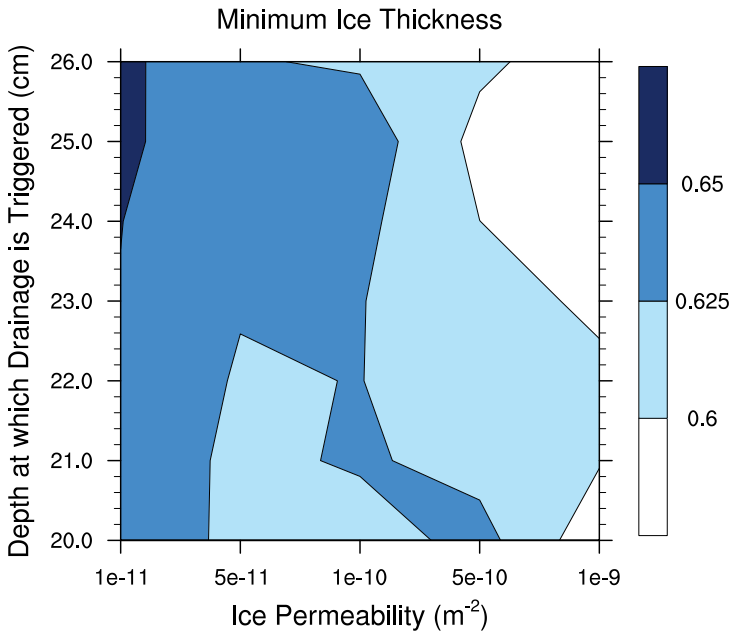

Figure 3.18: *Minimum ice thickness at the end of the simulation for varying permeability and trigger depth sensitivity parameters using 2009 forcing and topography.*

width of this "melting peak" is roughly 2 times larger in the CESM results as compared to the resolved model. Also, stage III is not represented at all in any of the CESM results, as there is no gradual rise in pond fraction after the ponds drain.

Figure 3.19 also shows the absorbed solar radiation (blue lines) for both models, as well as the total incident solar forcing (black line). In general, as pond fraction increases, the amount of absorbed solar radiation also increases due to the albedo reduction; therefore, more incident solar radiation is absorbed during times of high pond fraction as compared to times of low pond fraction. However, even though the two models show very different ponding behavior, the total integrated absorbed solar flux for the entire length of the simulation for each model was very close. Total absorbed shortwave flux for both models is shown in Table 1. The average absorbed solar radiation for CESM was only 38 Wm^{-2} larger than the average absorbed solar

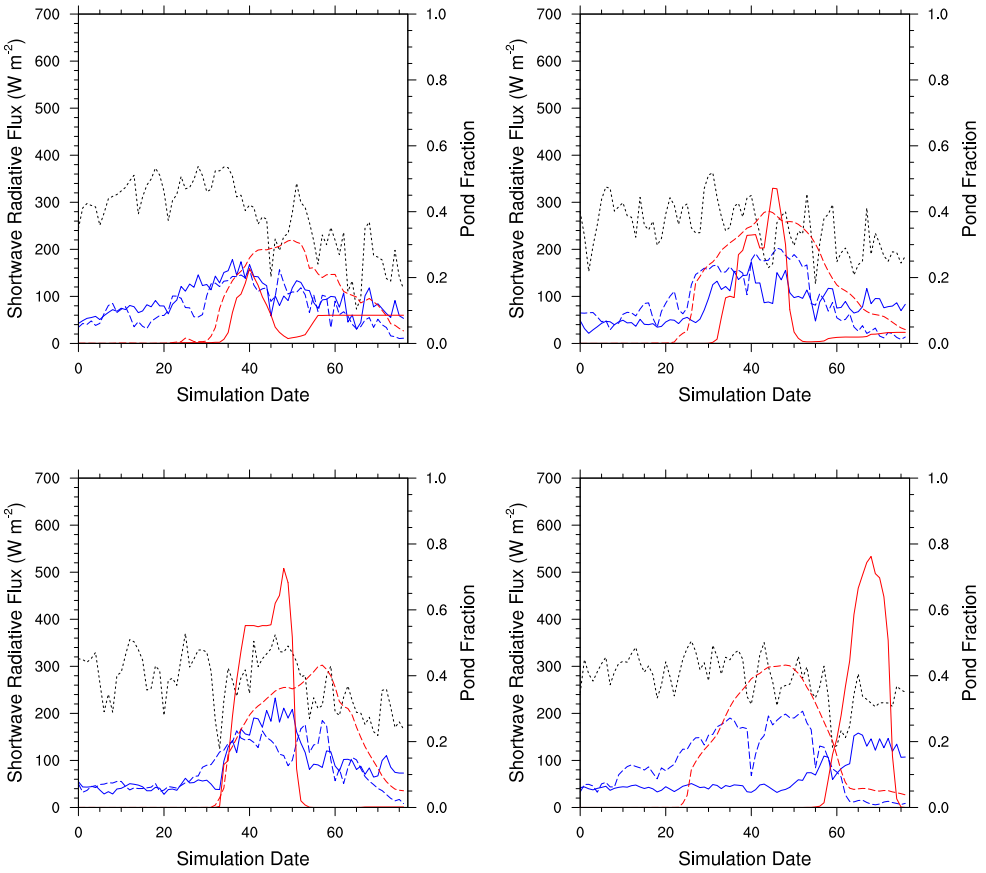

Figure 3.19: *Comparison of CESM ponding behavior to the ponding behavior of the resolved ice model forced with CESM forcing data. Dotted lines show data from CICE, solid lines show data from the resolved model. Red lines show pond fraction, and blue lines show absorbed shortwave radiation. Finally, the black dotted line represents total shortwave downwelling radiation. Simulation begins on May 5th.*

ratiation in the resolved model.

Fiigure 3.21 and Figure 3.22 show the albedo versus the pond fraction for the four years of both resolved model and CESM simulations, normalized by the total ice fraction. The resolved model figure is very similar to Figure 2.4, with a very linear, negative trend as pond fraction increases. The CESM figure, however, looks quite different. For each pond fraction, there are two corresponding albedos, indicating that although the pond fraction is the same, the albedo of the ice changes from stage

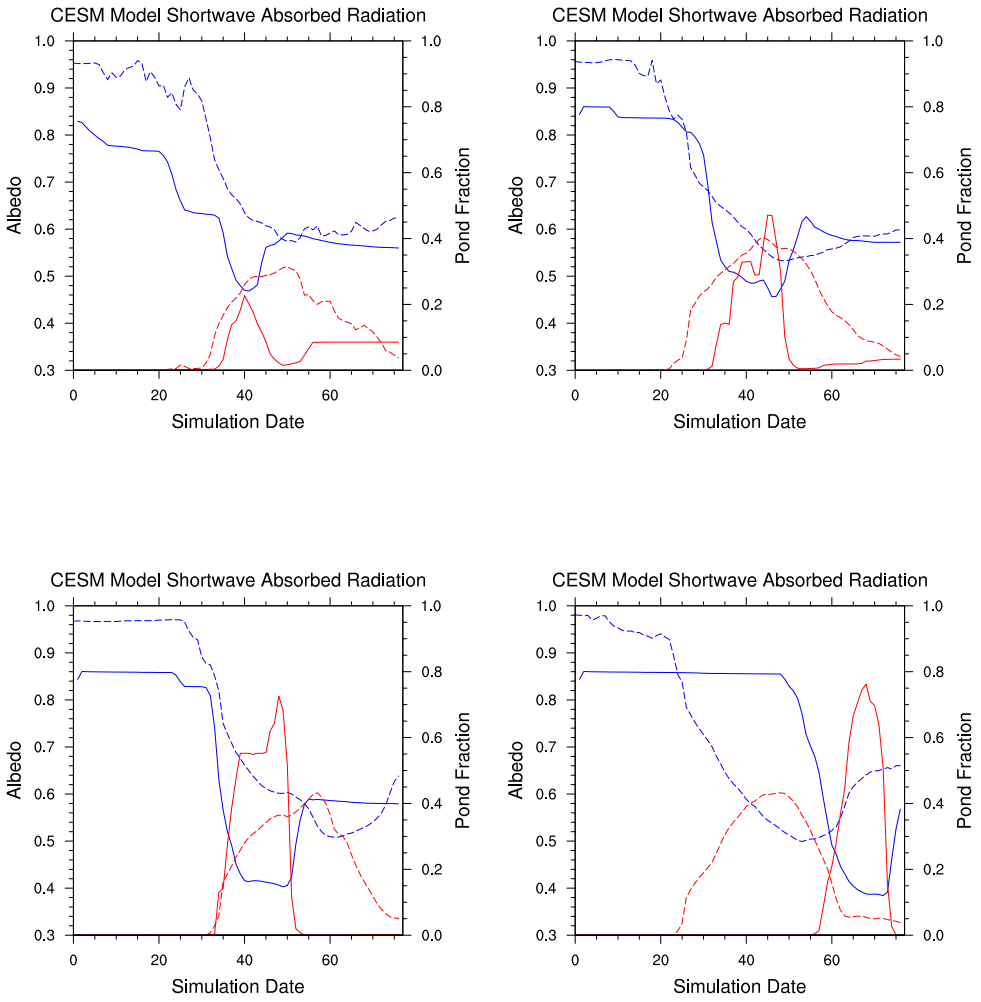

Figure 3.20: *Comparison of CESM albedo and pond fraction to the resolved ice model forced with CESM forcing data. Dotted lines show data from CICE, solid lines show data from the resolved model. Red lines show pond fraction, and blue lines show albedo. Simulation begins on May 5th.*

I to stage II of pond formation. This is confirmed by looking at a time series of model albedo, shown in Figure 3.20. Albedo steadily declines suggesting that other elements in CESM play a larger role in calculating the albedo of the ice than the melt pond fraction.

The pond fraction in the resolved model reaches a slightly smaller peak height

Year	CESM Total Integrated Absorbed Flux (Wm^{-2})	Resolved Model Total Integrated Absorbed Flux (Wm^{-2})
Year 1	763.3	625.7
Year 2	606.0	631.4
Year 3	715.3	661.6
Year 4	586.6	600.6

Table 1: Comparison of total absorbed shortwave flux for both the resolved model and CESM.

than both simulations with observational forcing (Figure 2.3), and true observational results [Polashenski et al., 2012]. To explain this difference, we hypothesized that in our search for a grid point in CESM that correctly matched the ice coverage around Barrow, AK, we moved far enough north that we picked a much colder grid point than Barrow during the summer months. Without correct temperature forcing, ponds may not form as quickly during the beginning of the simulation. To test this theory, we created a separate, hybrid forcing dataset consisting of all the CESM components listed before, except with the temperature replaced by warmer, observational temperature forcing. The resolved model was forced with this "warm" hybrid dataset, as well as with another "cold" hybrid dataset using CESM temperatures taken at a slightly higher level, and therefore slightly colder point, than the surface temperature. Results from these two runs are shown in Figure 3.23.

Using the warmer, observational temperature forcing not only caused the pond fraction to peak at a much higher value, but also shifted the onset date of ponding earlier by 10 days. This indicates that atmospheric temperature forcing plays an important role in determining how and when melt ponds form in the Arctic. Also, these results show a possible bias in how CESM generates melt ponds. Based on the

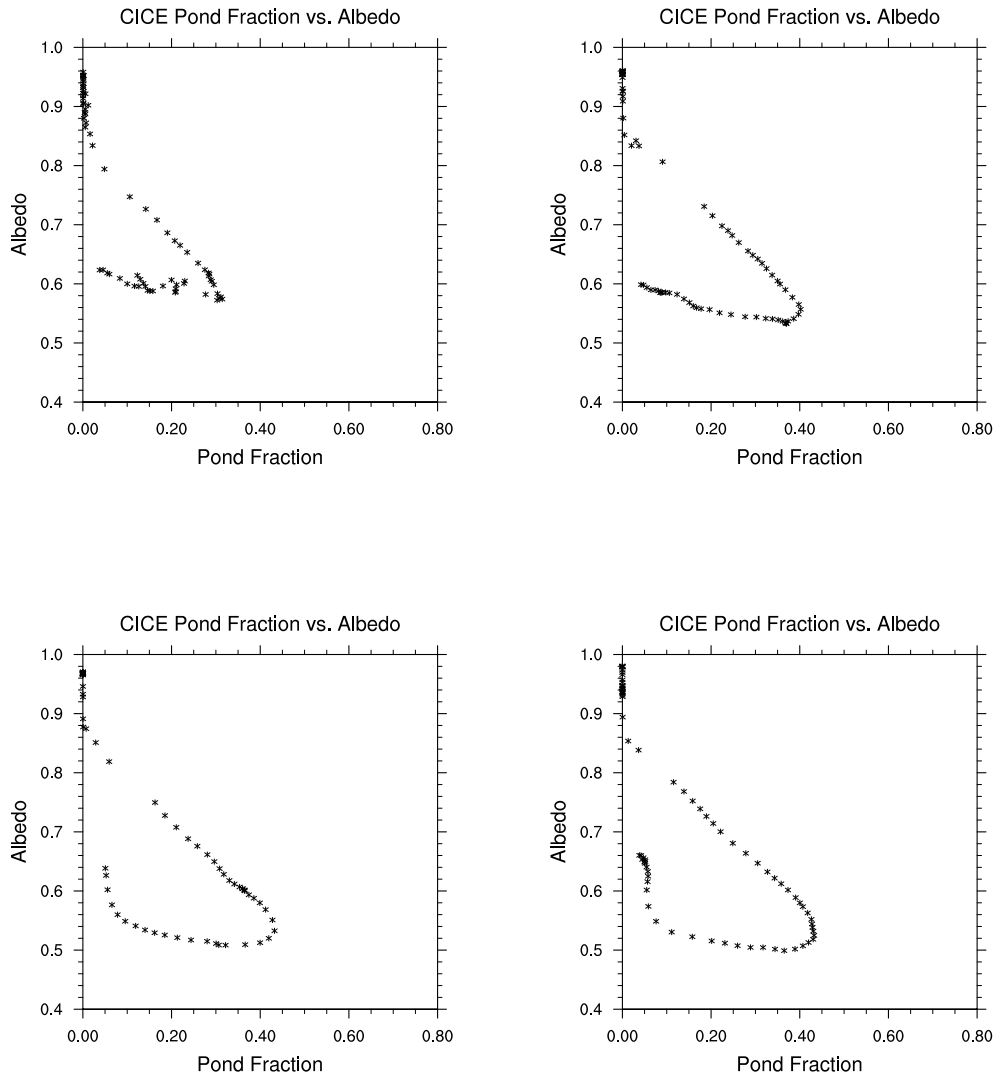

Figure 3.21: *Relationship between pond fraction and albedo for four years of CESM simulations. Albedo is normalized by the total ice fraction.*

resolved model, the forcing conditions at the grid point we picked should not generate ponds until 45 days into the simulation, around June 20. However, CESM creates ponds using this exact forcing nearly 30 days earlier. This indicates that the way in which CESM creates melt ponds is not realistic, and further research needs to be done to determine exactly what needs to be changed in order to better simulate realistic

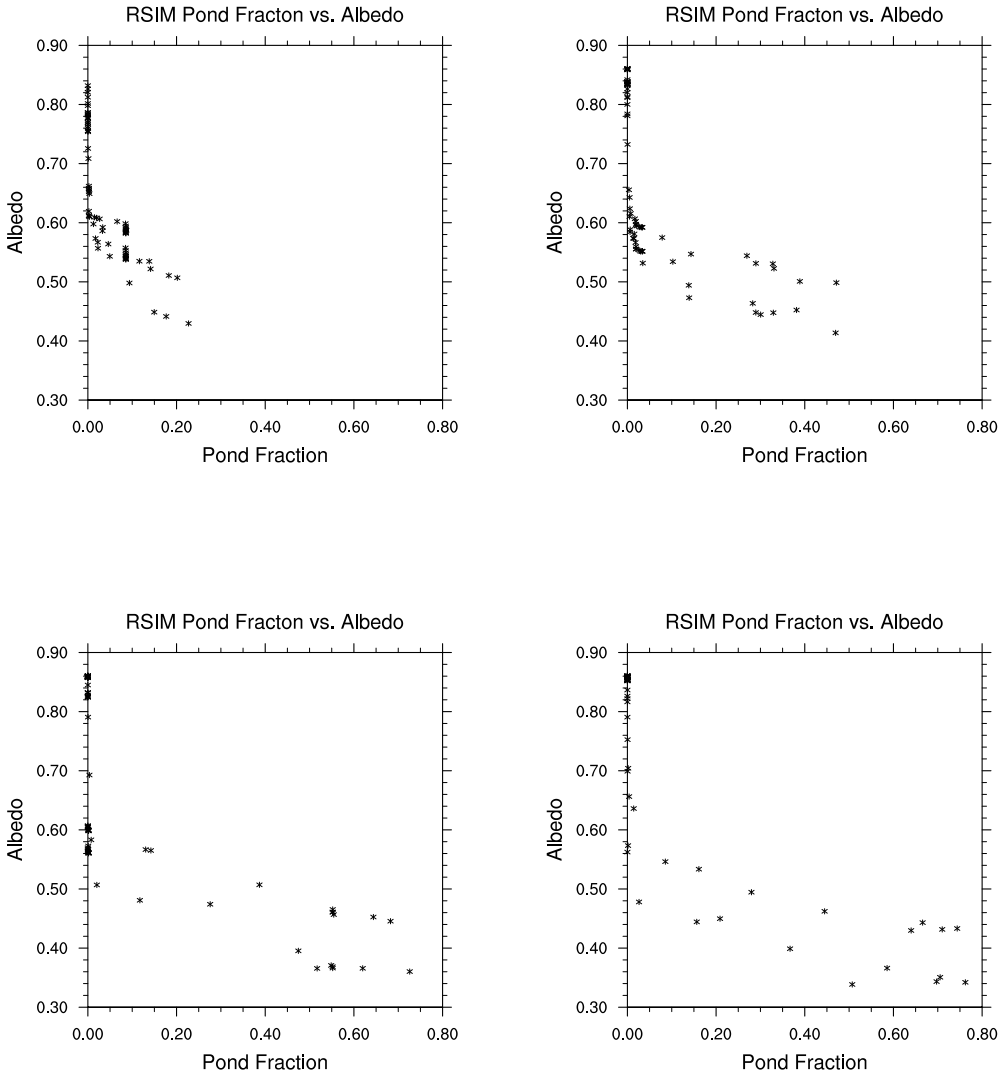

Figure 3.22: *Relationship between pond fraction and albedo for four years of resolved model simulations forced with input data from CESM.*

pond formation.

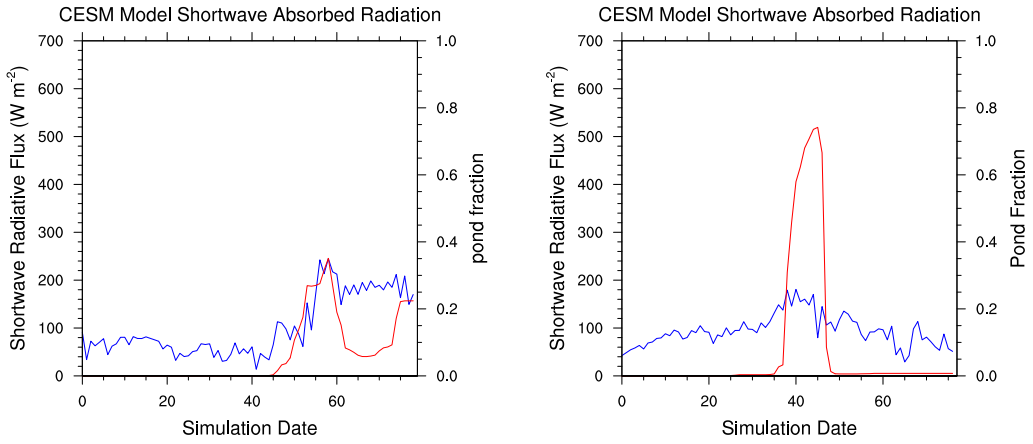

Figure 3.23: *Comparison of the resolved model forced with the "cold" dataset (left) and with the "warm" dataset (right). Increasing the temperature clearly shifts the melting peak earlier in the season and increases the maximum pond fraction that the simulation reaches.*

4 Conclusions

Conclusions from this work can be divided into three main categories. First, we assert that the ponding behavior in CESM looks far different from the behavior shown by our resolved ice model, and we present a possible area where improvement could be directed to improve pond parameterization in CESM. Second, we explore the effect of changes in initial snow depth on the end-date pond fraction, specifically through the mechanism of deep-channel formation early in the melt season. Finally, we show strong evidence that the trigger depth method for draining melt ponds, proposed by Chris Polashenski, properly simulates stage II of melt pond evolution: the drainage stage.

CESM Comparisons

Figure 3.19 shows that the pond evolution of the resolved ice model is much different from the pond evolution of CESM. The appearance of the melting peak does not follow the 3 stage method observed in field data, and the melting peak in CESM is much wider than in the resolved model.

Our comparisons show that the sea ice parameterization in CESM is responsible for much of the discrepancy between CESM and the resolved model. Using identical forcings, therefore eliminating any possible average melt-season shortwave forcing bias, it is clear that CESM creates ponds much differently than our resolved model, with a much wider melting peak. This results in a heat flux discrepancy between the two models that creates a temporal shift in the absorbed solar flux in CESM towards the end of the melt season. Our simulations show that correct pond formation should create a spike in absorbed solar flux near the beginning of the simulation (except in Year 4), due to the rapid rise in pond coverage. Further research needs to be performed to determine if Year 4 is an anomaly, or if this late-season melting is seen in other years.

Although the total integrated solar flux for both models is similar for each year tested (Table 1), the temporal shift and broadening of the absorbed flux peak could create errors in CESM later in the year. For example, delaying the majority of the absorbed solar flux could delay the ice break-up. This could affect the model in many ways, including changing the ocean currents and altering the surface heat budget.

Another alarming feature from CESM is the tremendous interannual variability

in the date of onset of melt ponds. Figure 1.3 shows that over the course of 14 years, the date of melt pond onset varies by nearly 50 days. Although observational data is limited, there are no indications currently that pond onset varies from year to year by over 10 days [Polashenski et al., 2012]. This tremendous range may contribute unnecessary amounts of variability to other elements of the model, such as absorbed solar flux (see Table 1), reducing its accuracy.

CESM creates melt ponds using a "thickness class" scheme, dividing each grid cell into five thickness classes, each representing a range of ice thicknesses. The percentage of the ice that exists in each thickness class defines the topography of the ice. Flat ice will have nearly 100% of the ice in one thickness class, while rough ice will have a large spread of percentages over all five classes.

Although analysis of the thickness class method is beyond the scope of this project, changing the use of this method could be one area of exploration in improving how CESM parameterizes melt ponds. Although CESM does not have the capability to resolve individual ponds, more than five thickness classes may be needed to accurately represent the changes in pond coverage that occur over as little as 12 hours [Polashenski et al., 2012]. Perhaps the usage of a probability density function to represent the pond fraction for each grid point could improve the behavior of the model without adding too many additional variables.

Snow Depth

Several interesting results were found by varying the initial amount of snow in the model. First, we discovered that the initial amount of snow impacts the date at which the ponds drain much more than it impacts the date at which the ponds form. Adding additional snow created diminishing returns on the pond formation date; these diminishing returns were not observed when studying the drainage date. Although this result may be in part simply a consequence of the model's coding, it is interesting to note that the minimum snow depth greatly affects the drainage behavior, an element of melt pond simulations that has not yet been studied closely. More research is needed to determine the exact correlation, but these results could be used to further improve the accuracy of melt pond models based on initial conditions such as snow depth.

We also determined that ponding at the end of the melt season is strongly controlled by the depth of the channels that have been carved in the ice throughout the summer, although Figures 3.17 and 3.18 show that permeability plays a role as well. Based on the results of this project, channels that are not deep enough to sit below the water table after the ponds have drained will never create late-season ponds. Therefore, the end-season pond fraction (and end-season surface energy budget) is mainly controlled by how deep these channels are carved during the early and middle stages of the melt season.

We show that the amount of snow on the surface of the ice plays a strong role in determining how deep these channels will form, and this relationship is very nonlinear.

Figure 3.10 shows that simply adding a few millimeters of snow on top of the ice between 4cm and 5cm minimum snow depth increases the minimum ice thickness by 30cm, creating much shallower channels, and decreasing the likelihood to form ponds at the end of the season.

This abrupt change in system behavior is due to the amount of ice that melts during the middle of the melt season. The ice albedo feedback is strongest during the period of highest pond fraction, usually 25-30 days into the melt season. If enough ice has not melted by the time the ponds drain, the surface topography remains flat and smooth, without deep channels for late-season ponds to form. With identical forcing, ice with deep snow is melted less than ice with shallow snow. Deep initial snowpack takes longer to melt enough to expose bare ice, allowing ponds to form. Once ponds form on bare ice, the ice-albedo feedback accelerates the melt around the ponds, allowing deep channels to be carved in the ice. By comparison, low initial snowpack exposes bare ice sooner in the melt season, allowing the feedback process to act for longer, and allowing deeper channels to be formed. The results of this work show that the maximum "minimum snow depth" that will still allow this feedback process to occur is between 3cm and 4cm (Figures 3.1 and 3.10), but depends on permeability.

We have shown that snow depth plays an important role in determining if ponds will form at the end of the melt season. This knowledge could help make predictions about the state of Arctic sea ice in future years and could be used in global climate models to better parameterize ponds based only on information about the snow depth. Also, as stated in the introduction, Arctic sea ice is gradually transitioning away from

multi-year ice to first-year ice. Because first-year ice is much flatter than multi-year ice, deep channels are less likely to form during the melting season. As meltwater spreads out on flat ice, it melts through the icepack evenly, rather than carving deep channels at only a few sites. As a result, first year ice may be less likely to form ponds later in the year, and could contribute to a slight damping effect on global warming by sustaining a high albedo for longer. These inferences are highly speculative, however, and much more research would be needed to confirm them.

Trigger Depth Confirmation

This work presents a new approach to controlling how and when melt ponds drain to sea level at the beginning of stage II of pond evolution. Many models do not employ a specific method to trigger the pond drainage. These models simply allow the permeability of the ice to increase gradually throughout the simulation, until a threshold permeability is reached that allows the accumulated meltwater to percolate through the ice.

Collaboration with Chris Polashenski revealed that the process for pond drainage is much more nonlinear than most current models assume. Instead of a gradual drain, observations show that drainage occurs rapidly: a single pond can completely drain to sea level in a matter of hours. Polashenski suggested that the temperature of the ice plays the largest role in determining when these ponds drain. Once the ice reaches a temperature of -0.5 °C, the permeability drastically increases, and ponds quickly drain. An element of uncertainty with this method is picking the depth at which to

measure this ice temperature, which is what we tested with this model.

Results show that using the trigger depth method for draining melt ponds produces drainage behavior very similar to field observations. This confirmation serves as a "proof-of-concept" for this approach, showing that it can be used in future models to correctly simulate drainage behavior. This work suggests that the depth at which the ice temperature should be measured to trigger drainage is 21cm below the ice. Although this result comes from only one model, using a limited set of sensitivity parameters, this depth could at least serve as a starting point for a future, more detailed investigation into this topic.

References

Bitz, Cecilia. Numerical modeling of sea ice in the climate system, lecture notes from ipy sea ice summer school in 2007, 2010.

Eicken, H.; Grenfell, T. C.; Perovich, D. K.; Richter-Menge, J. A., and Frey, K. Hydraulic controls of summer arctic pack ice albedo. *Journal of Geophysical Research: Oceans*, 109(C8), 2004. ISSN 2156-2202. doi: 10.1029/2003JC001989. URL http://dx.doi.org/10.1029/2003JC001989.

Fetterer, F.; Knowles, K.; Meier, W., and Savoie, M. Sea ice index. boulder, colorado usa: National snow and ice data center. digital media, 2002.

Freitag, J. and Eicken, H. Meltwater circulation and permeability of Arctic summer sea ice derived from hydrological field experiments. *Journal of Glaciology*, 49(166): 349–358, 2003.

Golden, K. M.; Eicken, H.; Heaton, A. L.; Miner, J.; Pringle, D. J., and Zhu, J. Thermal evolution of permeability and microstructure in sea ice. *Geophysical Research Letters*, 34(16), 2007. ISSN 1944-8007. doi: 10.1029/2007GL030447. URL http://dx.doi.org/10.1029/2007GL030447.

Intergovernmental Panel on Climate Change (IPCC), . *Climate Change 2007: The Physical Science Basis. Contribution of Working Group I to the Fifth Assessment Report of the Intergovernmental Panel on Climate Change*. Cambridge Univ. Press, 2013.

Kay, Jennifer E.; Holland, Marika M., and Jahn, Alexandra. Inter-annual to multi-decadal arctic sea ice extent trends in a warming world. *Geophysical Research Letters*, 38(15), 2011. ISSN 1944-8007. doi: 10.1029/2011GL048008. URL http://dx.doi.org/10.1029/2011GL048008.

Lüthje, M.; Feltham, D. L.; Taylor, P. D., and Worster, M. G. Modeling the summertime evolution of sea-ice melt ponds. *Journal of Geophysical Research: Oceans*, 111(C2), 2006. ISSN 2156-2202. doi: 10.1029/2004JC002818. URL http://dx.doi.org/10.1029/2004JC002818.

Marshall, John and Plumb, Alan. *Atmosphere, Ocean, and Climate Dynamics: An Introductory Text*. Academic Press, 1st edition, 2008. ISBN 978-0125586917.

Perovich, Donald K. and Elder, Bruce. Estimates of ocean heat flux at sheba. *Geophysical Research Letters*, 29(9):58–1–58–4, 2002. ISSN 1944-8007. doi: 10.1029/2001GL014171. URL http://dx.doi.org/10.1029/2001GL014171.

Petrich, C.; Eicken, H.; Polashenski, C.; Sturm, M.; Harbeck, J., and D. K.and FinneganPerovich, D. C. Snow dunes: A controlling factor of melt pond distribution on arctic sea ice. *J. Geophys Res.*, 2012. doi: 10.1029/2012JC008192.

Polashenski, C.; Perovich, D., and Courville, Z. The mechanisms of sea ice melt pond formation and evolution. *Journal of Geophysical Research: Oceans*, 117(C1), 2012. ISSN 2156-2202. doi: 10.1029/2011JC007231. URL http://dx.doi.org/10.1029/2011JC007231.

Polashenski, Chris. 2011 summer healy icescape project. http://chrispolashenski.com/photos.php, 2011.

Roe, Gerard. Feedbacks, timescales, and seeing red. *Annual Review of Earth and Planetary Sciences*, 37(1):93–115, 2009. doi: 10.1146/annurev.earth.061008.134734.

Rothrock, D. A.; Yu, Y., and Maykut, G. A. Thinning of the arctic sea-ice cover. *Geophysical Research Letters*, 26(23):3469–3472, 1999. ISSN 1944-8007. doi: 10.1029/1999GL010863. URL http://dx.doi.org/10.1029/1999GL010863.

Scott, F. and Feltham, D. L. A model of the three-dimensional evolution of arctic melt ponds on first-year and multiyear sea ice. *Journal of Geophysical Research: Oceans*, 115(C12), 2010. ISSN 2156-2202. doi: 10.1029/2010JC006156. URL http://dx.doi.org/10.1029/2010JC006156.

Skyllingstad, E. D.; Shell, K. M., and Collins, L. Simulation of the melt season using a resolved sea ice model with snow cover and melt ponds. *J. Geophys Res. In Preparation*, 2013.

Skyllingstad, Eric D. and Paulson, Clayton A. A numerical study of melt ponds. *Journal of Geophysical Research: Oceans*, 112(C8), 2007. ISSN 2156-2202. doi: 10.1029/2006JC003729. URL http://dx.doi.org/10.1029/2006JC003729.

Skyllingstad, Eric D.; Paulson, Clayton A., and Perovich, Donald K. Simulation of melt pond evolution on level ice. *Journal of Geophysical Research: Oceans*, 114(C12):n/a–n/a, 2009. ISSN 2156-2202. doi: 10.1029/2009JC005363. URL http://dx.doi.org/10.1029/2009JC005363.

Ströeve, Julienne C.; Kattsov, Vladimir; Barrett, Andrew; Serreze, Mark; Pavlova, Tatiana; Holland, Marika, and Meier, Walter N. Trends in arctic sea ice extent from cmip5, cmip3 and observations. *Geophysical Research Letters*, 39(16), 2012. ISSN 1944-8007. doi: 10.1029/2012GL052676. URL `http://dx.doi.org/10.1029/2012GL052676`.

Trenberth, K. E.; Fasullo, J. T., and Kiehl, J. Earth's global energy budget. *Bull. Amer. Meteor. Soc.*, 90:311–323, 2009.

University of Alaska, Fairbanks, . Barrow sea ice thickness and sea level. http://seaice.alaska.edu/gi/observatories/barrow_sealevel, 2012.